INAF

ISTITUTO NAZIONALE DI ASTROFISICA

NATIONAL INSTITUTE FOR ASTROPHYSICS

Publication Year	2019
Acceptance in OA@INAF	2023-02-21T13:43:57Z
Title	ALTA Center: Advanced LBT Turbulence and Atmosphere Center Report 12/2019
Authors	MASCIADRI, Elena; TURCHI, Alessio
Handle	http://hdl.handle.net/20.500.12386/33665

5   Milestone 3: Development and deployment of the optical turbulence prediction with corresponding data access capabilities from LBTO

The third phase of our study has been dedicated to the model setting-up for the forecast of the optical turbulence (OT). As said in Section 2, to forecast the optical turbulence we need the Astro-Meso-Nh code that has been conceived and developed exactly for this goal. Differently from the atmospheric parameters, a calibration of the model is necessary. This means to fix a free parameter in the code that is related to the turbulence kinetic energy. The model calibration is a technique proposed originally by Masciadri & Jabouille 2001, A&A [13]. The same principle has been used later on by several authors with mesoscale models who implemented the same method or modified versions of the original one ([14],[15],[16],[17], etc.). From a practical point of view, to calibrate an atmospherical model a rich statistical sample of observations of the vertical distribution of the OT i.e. the C_N^2 profiles is necessary. We used for the model calibration measurements of the C_N^2 obtained with a Generalised SCIDAR (Fig.40) during intense site testing campaigns that has been carried out by our team on the period 2005-2008 at Mt.Graham and consisting on 43 nights distributed in different periods of the solar year. However we rapidly realised that the usual calibration could not provide useful results as in LBT the unique observations that are performed routinely at present time and that can be used as a reference in whatever instant are the measurements obtained with a DIMM. The typical seeing measured by the DIMM did not matched with the typical seeing measured by the SCIDAR. This was not surprising as the difference might be justified in many ways: the SCIDAR run for a limited number of nights and the DIMM run inside a dome. Moreover the DIMM provides measurements of the seeing i.e. the integrated value of the C_N^2, it is not a vertical profiler. This should not be a problem in principle as it is possible to compare the observed with the simulated seeing but it was necessary to conceive a different method of calibration of the model. The problem is however that the DIMM is located inside the LBT dome (see Fig.41) and it is therefore basically impossible that a model calibrated using observations that are independent on the dome seeing can match with measurements affected by the dome seeing. On the other side it was not possible to disentangle the contribution provided by the dome from that coming from the atmosphere[7].

After an extended analysis of the problem we arrived at the conclusion that the real useful information from the astrophysical point of view was to provide a right estimate of the seeing arriving at the focus of the telescope. The DIMM inside the dome is therefore not a real problem if we change our perspective. It can be considered as an added value instead of a problem. We can not know the turbulence contribution of the pure atmosphere but we have a good reference of the total turbulence that arrives on the detector. Obviously the choice done followed a very pragmatical point of view. We chose the solution that permitted us to provide an answer to the observational necessities.

We though therefore to an alternative method to calibrate the model that could take into account the simultaneous information from the DIMM and from the Generalised SCIDAR. A method that could use as a reference the total turbulence as observed by the DIMM.

Such a method has some pro and cons. The pros is that we can forecast the turbulence that arrives directly on the CCD. This approach has also the advantage that we can count on a rich statistics for the part of the turbulence that is mostly relevant from a quantitive point of view that is the turbulence close to the ground as this is provided by the DIMM. The cons is that we reconstruct a C_N^2 that contains the dome contribution. It is not a cons by itself but we have to be aware about that.

Which may be the effect on the other astroclimatic parameters (θ_0 and τ_0) ? The isoplanatic angle is mainly affected by the turbulence in the free atmosphere and the dome contribution is basically not relevant for θ_0. We expect that the wind speed inside the dome should be relatively small and almost zero as the air is confined inside the dome. Because of that, we expect that also in the case of the τ_0 the contribution should not be very important.

---

[7]A dedicated plan for monitoring of the dome seeing has been traced by the LBTO Director, C. Veillet for the next future

Figure 40: Generalised SCIDAR mounted at the focus of the Vatican Advanced Technological Telescope (VATT), telescope of 1.8 m located close to the LBT on the summit of Mt.Graham

DIMM
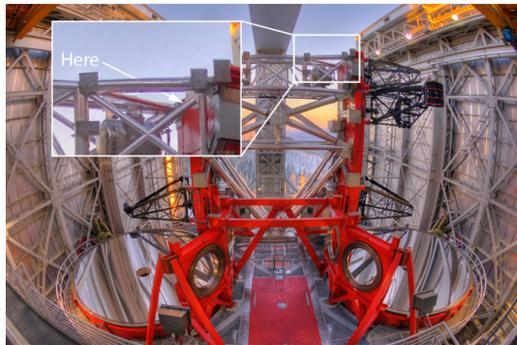
Figure 41: Vision of the internal part of the LBT dome. The zoom on the top right indicate the position of the DIMM

Anyway, using the configuration that we selected and that we have just described we calibrated the model and we then validated it. Preliminary results of the new calibration method performed on a sample of 42 nights (21 in summer and 21 in winter) uniformly distributed on a solar year. Results have been presented at the Conference LBT Users' Meeting (2017) in Florence. In this phase we could verified that the method could work. On beginning of 2018 we completed a more precise calibration on a much richer sample of nights (102) uniformly distributed along a solar year. Finally we implemented the new calibration in the operational ALTA system. Since beginning of 2018 the operational system with the new calibration method is running nightly at LBT. We highlight that a procedure of calibration consists on:

1. performing a set of simulation related to X nights (X has to be statistical relevant) with the non calibrated model;
2. performing the calibration i.e. calculating the free parameters;
3. performing agin the simulations related to the same X nights with the calibrated model.

We do not enter in the details of the calibration procedure as this can be subject of a paper but we present

the results that quantify the reliability of the model.

5.1   Model calibration

We summarise with the following images, the main conclusions obtained in this first phase of the study. Fig.42 shows the average C_N^2 profile as observed and forecasted by the 43 nights in which it is visible the good correlation on the typical vertical distribution on the atmosphere. The GS bump at h = 0 km is the result of the natural intrinsic resolution of the instrument at that height that does that some turbulence is seen under ground. We can not expect therefore that the shape of the C_N^2 measured and simulated matches at h = 0 km. A model works indeed in a completely different way. What we have to do at those heights is to compare mot the shape but the integral of the measured and simulated turbulence in the vertical slab equivalent to the resolution of the instrument. When we look at the vertical profiles we can count only on a sample of 43 nights as there is no an automatic vertical profiler at Mt.Graham.
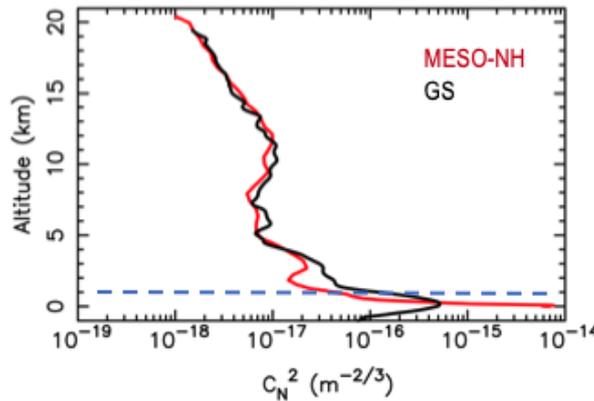
Figure 42:   Average C_N^2 profile obtained with a sample of 43 nights. Black line: observations from the GS; Red line: forecasts from the Astro-Meso-Nh. The blue dash line separate the regions in which the SCIDAR and the DIMM impact on the calibration.

Fig.43 shows the results of the model calibration i.e. the scattering plot of observed and simulated seeing on the rich sampling of 102 nights. A similar scattering plot is calculated for the sub-samples related to the summer and winter time. We define summer: [April - September] and winter: [October - March]. The sample has been identified by taking a number of nights uniformly distributed in a solar year: 2016. The good correlation of the forecasted seeing with measurements tells us that the calibration strategy is reliable. We highlight that we consider the seeing extended up to 1.5" as values larger than this threshold are not interesting in terms of science operations. As can be see in the figure, in general, the larger is the seeing the larger is the dispersion between observations and forecasts.

Fig.44 shows the histogram and the cumulative distribution of the seeing observed with the DIMM and forecasted by the model on the sample of 102 nights. Fig. 45 and Fig. 46 show the same in the summer and winter period. Those results indicate that the statistics of the turbulence is well reconstructed by the model on the whole wear as well as on the summer and winter period. The medium value of the seeing does not show a significant difference between summer and winter period. This is also confirmed by the climatological analysis performed in ALTA Center by calculating the cumulative distribution of DIMM measurements in the last years (see link 'Climatology' on the main Menu). The median values of the seeing in winter and summer time is mostly comparable with small fluctuations that do not show a significative difference in the two seasons. The shape of the histograms in Fig.44, Fig.45 and Fig. 46 is however slightly different. During the winter time we observe a larger frequency of high value of the seeing with respect to the summer time. This is not surprising as
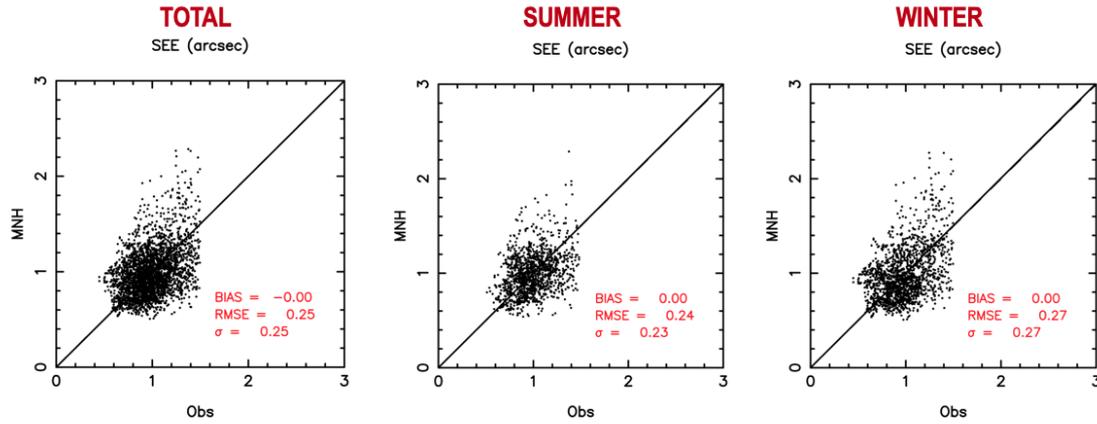
Figure 43: **Calibration sample**: Scattering plots of the seeing observed and simulated by the Astro-Meso-Nh model in the total 102 nights (left), summer (center) and winter (right).
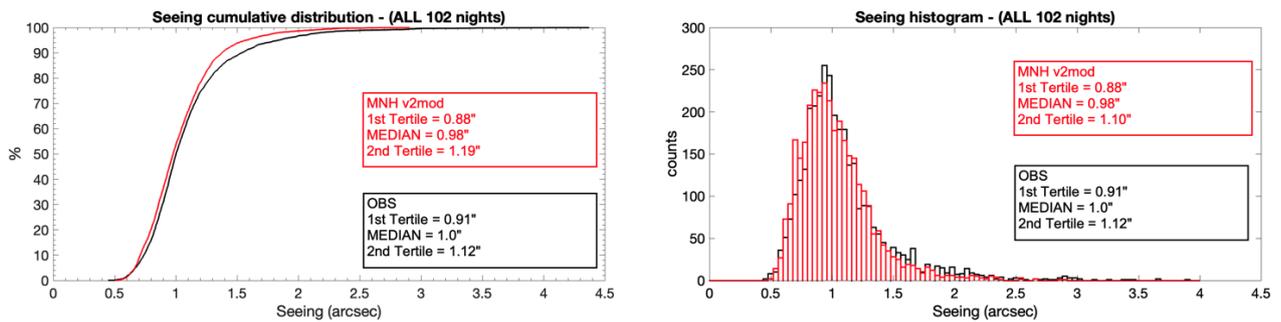
Figure 44: **Calibration sample**: cumulative distribution and histograms of the seeing obtained taking into account the sample of 102 nights as observed (DIMM) and reconstructed by the Astro-Meso-Nh model.

the seeing value is mainly driven by the boundary layer and we know that the wind speed close to the ground can reach burst more frequently than in winter time (see the queue of the histograms of Fig.4 and Fig.5 in [7]). We note that in winter time the median is 7.5 ms^{-1} while in summer time is 5.6 ms^{-1} ([7]) but this visibly does not impact on the seasonal trend of observed seeing. This lets us think that the fact that the seeing is measured inside the dome can have an impact on this.

5.2 Model validation

For the model validation we selected a sample completely independent from the calibration one. All the nights belong to the solar year 2018. Fig.47 show the scattering plot of the seeing in the whole sample, in summer and winter time. Fig.48, Fig.49 and Fig.50 show the associated cumulative distribution and histograms. From a statistical point of view the the cumulative distribution and the histograms are very similar to the calibration one. If we look the scattering plot, the RMSE is slightly larger than in the calibration sample as the RMSE increases from 0.25" to 0.3". We note that at Cerro Paranal we obtained a slighter smaller value for the RMSE = 0.24". At present we have no enough element to indicate with certitude the cause of such a difference but we have to highlight that the seeing conditions are not the same in the two sites and, among others, the references that we used for the model calibration is not the same. In one cases we used instruments measuring turbulence
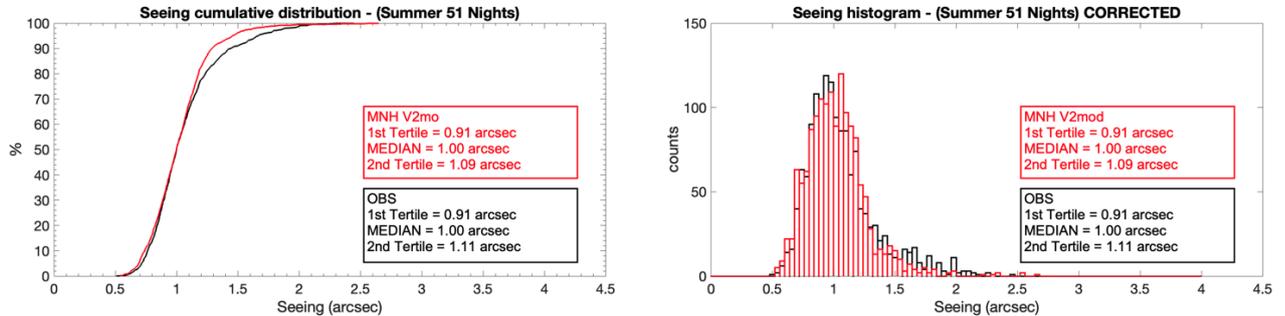
Figure 45: **Calibration sample**: cumulative distribution and histograms of the seeing obtained taking into account the sample of 51 nights in **summer** time as observed (DIMM) and reconstructed by the Astro-Meso-Nh model. Summer: [April - September].
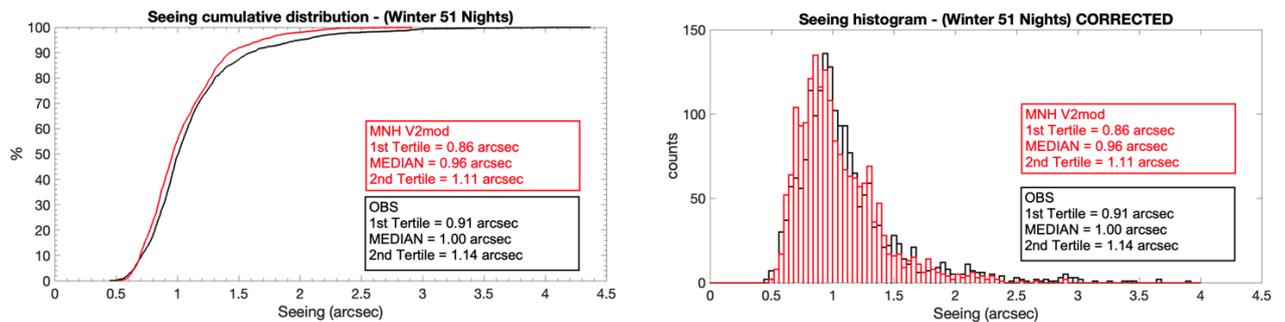
Figure 46: **Calibration sample**: cumulative distribution and histograms of the seeing obtained taking into account the sample of 51 nights in **winter** time as observed (DIMM) and reconstructed by the Astro-Meso-Nh model. Winter: [October - March].

in the pure atmosphere, in the other one we used a DIMM that is running inside the dome. It is worth to say that it is planned the purchase of a further DIMM that will be able to run on top of Mt.Graham and that might be included in the process of the forecast. It is possible therefore that the employment of the two DIMMs (one in open air and the other inside the dome) might help to improve the model performances.

A consideration on the validation sample is to be done. We collected a total of 229 nights i.e. all the nights with seeing measurements of the year 2018 (see [6] - Appendix A) . The fact that the number of nights is not 365 is mainly due to the fact that measurements are performed with the LBT-DIMM located inside the LBT dome. This means that when the dome is close for whatever reason, measurements are missed. If we consider the shutdown period of LBT (1.5 months in July–August) plus the number of nights lost because of bad weather in 2018 and we subtract that to the total number of 365 in 1 yr, we find the number of nights 229 that we treated for the validation period that corresponds to the allocated time of LBT on 2018 ($\sim$ 64 per cent of the total time).

On Fig.51 is shown a selection of the temporal evolution of raw DIMM observations and the raw forecasts from the model. It is possible to see that not always the forecast respects the observations. For example, on the bottom right is shown a night in which the seeing in the first part of the night was mainly underestimated by the model. This means that sometimes the forecast can have a more important error. At this stage it is difficult to say which can be the cause of this disagreement. Possible causes of these discrepancies can be:
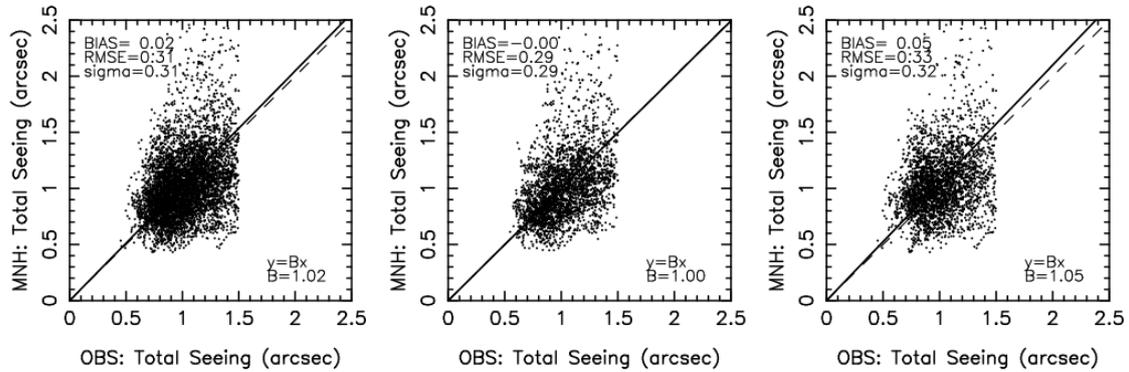
Figure 47: **Validation sample**: Scattering plots of the seeing observed and simulated by the Astro-Meso-Nh model in the whole validation sample (left), summer (center) and winter (right).
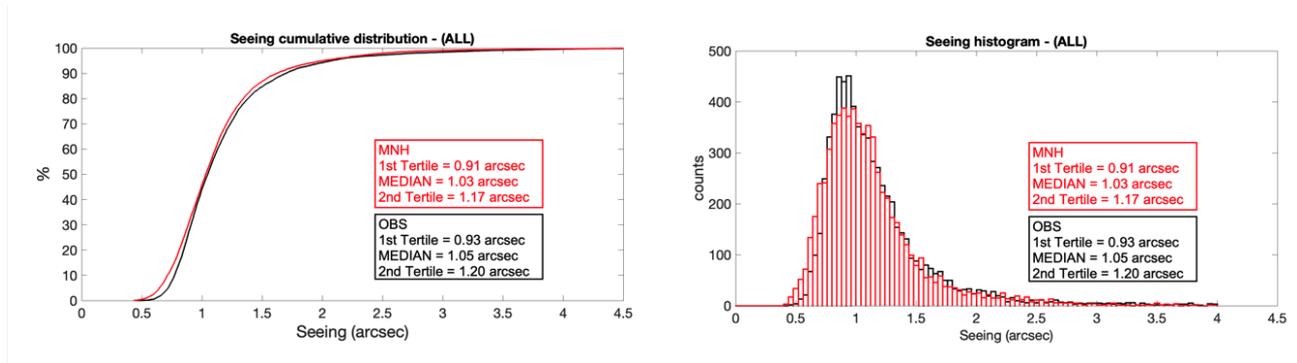
Figure 48: **Validation sample**: cumulative distribution and histograms of the seeing obtained taking into account the whole validation sample as observed (DIMM) and reconstructed by the Astro-Meso-Nh model.

1. Limitations of the parameterisation of the model;

2. Excess of seeing in the dome. The model is calibrated taking into account the dome seeing but this is done in statistical terms; On individual nights we can not exclude a difference between forecasted and observed value due to the dome contribution;

3. Initialisation data that can be not so representative some time. Of course if during a night the forecast of the GCM is poor, it follows that the mesoscale forecast will be poor too.

We think that when the seeing retrieved from SOUL will be available we will be able to deduce further insights in this respect. This might help us in understanding the origin of these kind of problems. Besides we will be forced to see if some different references in the model calibration have to be taken.

More recently we started to work on a new method aiming to improve the forecasts on a short time scale (order of a few hours) using a an auto-regressive technique. This time scale is by far the most critical for the routinely LBT observations. We decided therefore to start to work on this approach to try to provides some advantages to the astronomical community. We refer the readers to Section 7.1 for more details on this topic.
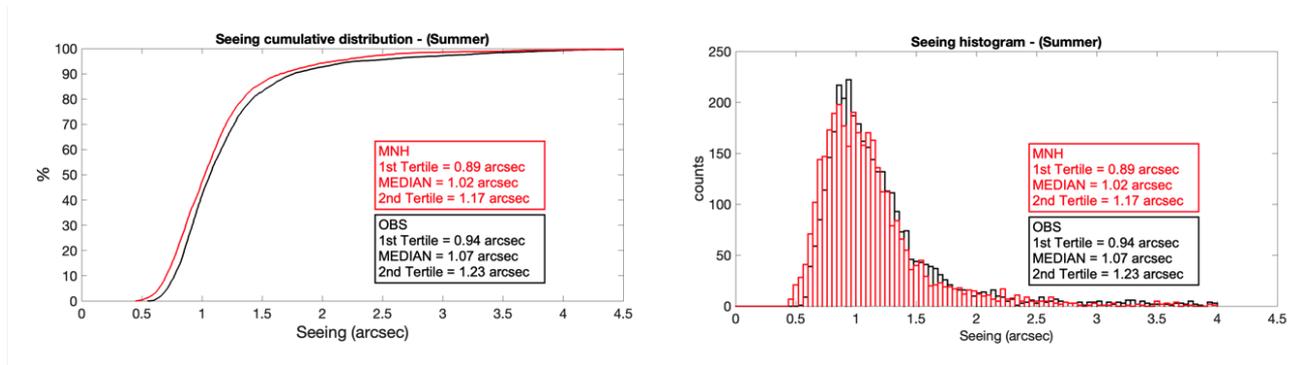
Figure 49: **Validation sample**: cumulative distribution and histograms of the seeing obtained taking into account the nights in the summer time as observed (DIMM) and reconstructed by the Astro-Meso-Nh model.
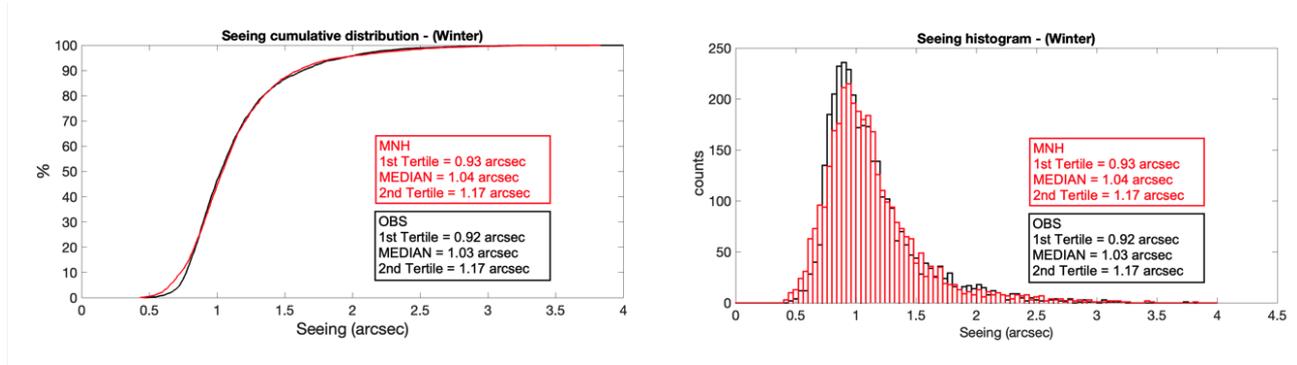
Figure 50: **Validation sample**: cumulative distribution and histograms of the seeing obtained taking into account the nights in the winter time as observed (DIMM) and reconstructed by the Astro-Meso-Nh model.

5.3 Technical developments

As we said in other passages of this report, the ALTA Center is by definition in continuous evolution. This is an intrinsical feature of all the atmospherical models whose performances depend on a set of elements such as the algorithms describing the physical phenomena, the initialisation data, the orography, the description of the ground (vegetation, lakes, etc). All this elements have to constantly be phased among them. For example, if the GCMs introduce some changes in the initialisation data coming out from these models we have to take care that the new products can still be read by the mesoscale model. If the mesoscale model (in our case Meso-NH) evolves i.e. if it is delivered with successive versions, we have to take care to phase the code Astro-Meso-Nh with the master version of the model that means to be able to run the Astro Meso-Nh code joint with the master, verify that the modifications in the master do not have important effects on the Astro Meso-Nh. If there are important changes in the codes, we have to verify which are the impacts on the parameters of our interest. We might define all this with a general expression such as *"support of the forecast system"*. We say that just to get clear that, the development and the run of an atmospherical model implies some not negligible work that guarantees that the automatic system can supply the required information and that this is continuously reliable.

During the 5 years contract we had to carry out a set of technical work that substantially permitted to ALTA Center to continue to run with its quantified performances and sometime even to improve them. We mention here the main ones:

(1) On July 2016 we switched to the master version MNH 5.2.1. We have therefore to phase Astro Meso-Nh
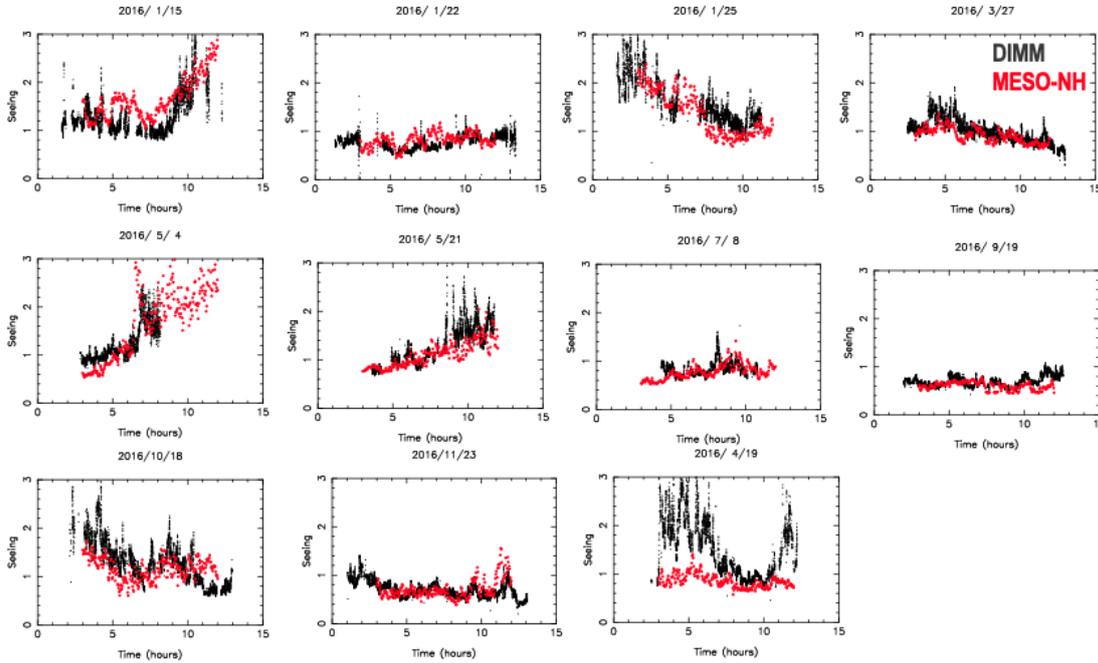
Figure 51: Selection of nights in which is shown the temporal evolution of the seeing as measured by the DIMM and the seeing as forecasted by the model.

to the new master version

(2) On November 2016, ECMWF offered as a possible output the new grid O1280 that was delivered for free. The reduced gaussian originally used was not any more available. Such a grid has a different sampling of the grid points on each latitude circle with respect to the reduced gaussian (previous one). The reduced gaussian characteristics is that to have the same horizontal resolution for all the latitude. In reality, because of constraints imposed by the Fast Fourier Transform, it offer constant resolution in blocks of latitudes, creating some jumps when the gradient is calculated. The O1280 grid permits to smooth out such an effect. The feature was not not fundamental for our application but, as it was free, we switched on the O1280 taking care to verify that simulations outputs obtained with Meso-Nh did not show differences. To use the O1280 we had to modify the master version of Meso-Nh

(3) On December 2016 we modified the C_N^2 algorithm of Astro-Meso-Nh accordingly to Masciadri et al. [17]. As a consequence, all the 2D maps of the astroclimatic parameters depending on the C_N^2

(4) On September 2017 the whole part of the code managing the production of figures to be displayed on ALTA Center has been translated from IDL to Python.

(5) On February 2018 the model configuration has bene changed for the configuration at high horizontal resolution (i.e. that with four domains and a maximum resolution of 100 m) so to be able to run on just 29 vertical levels.

(6) On February 2019 we switched from O1280 to gaussian regular. The decision was taken as the method permitting Meso-Nh to run with the O1280 was particularly heavy. The regular gaussian is based on the principle to have the same number of grid points for each latitude circle. It is characterised by a resolution increasing from the Equator to the Poles. Because of the limited extension of the domains such a feature is irrelevant for

our applications. We had however to verify that all the outputs of our simulations performed with the new data-set provided equivalent outputs from a statistical point of view.

(7) On March 2019 the new autoregressive method AR (see Section 7) has been implemented in the automated version of the code including the creation of the new metadata ouputs for the AR method.

(8) Implementation of a method that switch automatically the calibration version (summer and winter) at the right time.

6 Milestone 4: Automated meta-data archival

As indicated in Fig.1 the ALTA Center automatic forecast system includes the transmission of metadata to LBTO. With the term "metadata" we mean the temporal evolution of the forecasted values of all the parameters that are extracted from the forecasted 3D data cube in the coordinates of the LBT. We retrieved therefore the informations related to a specific point: (32.701309059 N, 109.889063 W).

Since April 2019 ALTA Center provides forecasts at different time scale, more precisely it provides forecasts in two configurations:

Forecast at long time scales: we mean with that the forecasts displayed early afternoon (14 LT) of the night before and extended for the whole successive night - black-line in Fig.11

Forecast at short time scales: when the night starts, at each full hour ALTA provides a forecast of the main parameters extended on the successive four hours. These forecasts are up-graded each full hours during the nights - red line in Fig.11

The user can visualise the outputs through the web-site of ALTA Center ($http : //alta.arcetri.inaf.it$). At the same time, the metadata of those forecasts are transmitted automatically through the network to LBTO. More precisely, metadata are located by the ALTA team on a protected web site and downloaded from the web-site by the LBTO team. The whole process is automatic and it has been synchronised. Once downloaded, the metadata are then injected in three different channels as indicated in Fig.52: **(1)** the LBT control room monitors, **(2)** the LBT telemetry tool and **(3)** the Science Operation tool to be used for the management of the astrophysical observations of LBT.

The metadata we are dealing about are the temporal evolution of temperature, wind speed, wind direction and relative humidity close to the surface (at the model levels corresponding to the heights of the sensors located on the top of the LBT dome), the PWV and the seeing. Further parameters (such as the isoplanatic angle (θ_0) and the wavefront coherence time (τ_0) will follow as soon as it will be possible to validate the forecasts with measurements provided by a MASS. During the night, at each full hour, the metadata related to the forecasts at short time scales are up-graded and automatically injected in the three channels cited above i.e. the Science Operation tool, the control room monitors and the telemetry tool.
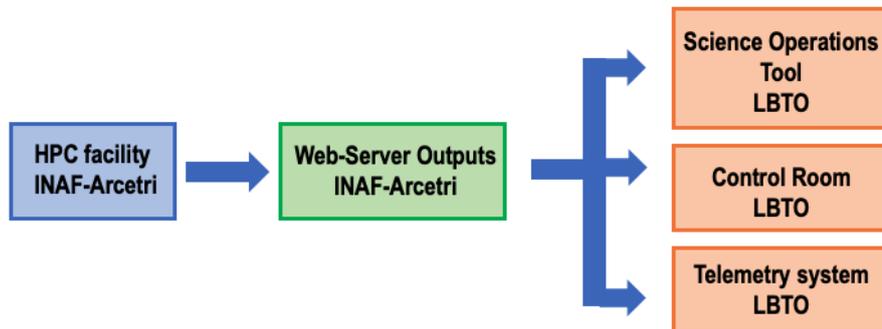
Figure 52: Flowchart of metadata transmission from INAF-OAA to LBTO. INAF-OAA posts metadata on the web-site and LBTO downloads data from the web-site. The whole process is completely automatic and synchronised.

The metadata transmission developed in a two step phases. On July 2016 a first automatic transmission system has been implemented in INAF-Arcetri allowing the transmission of a first release of metadata i.e.

the temporal evolution of the main atmospheric parameters close to the ground. These metadata have been organised by LBTO so be displayed in the control room of the telescope. On 2019, after the implementation of the forecasts at short time scale employing the autoregressive method, we developed a complete version of the automatic metadata transmission system that implied a more sophisticated transmissions procedure that up-grades data during the time. LBTO has been in charge to inject the metadata coming out from ALTA and inject them the telemetry system and the Science Operations tool. Fig.53 shows the LBT system status as seen through the web. In the red picture appears the link to ALTA to indicate that ALTA is now perfectly integrated on the LBTO operations system.
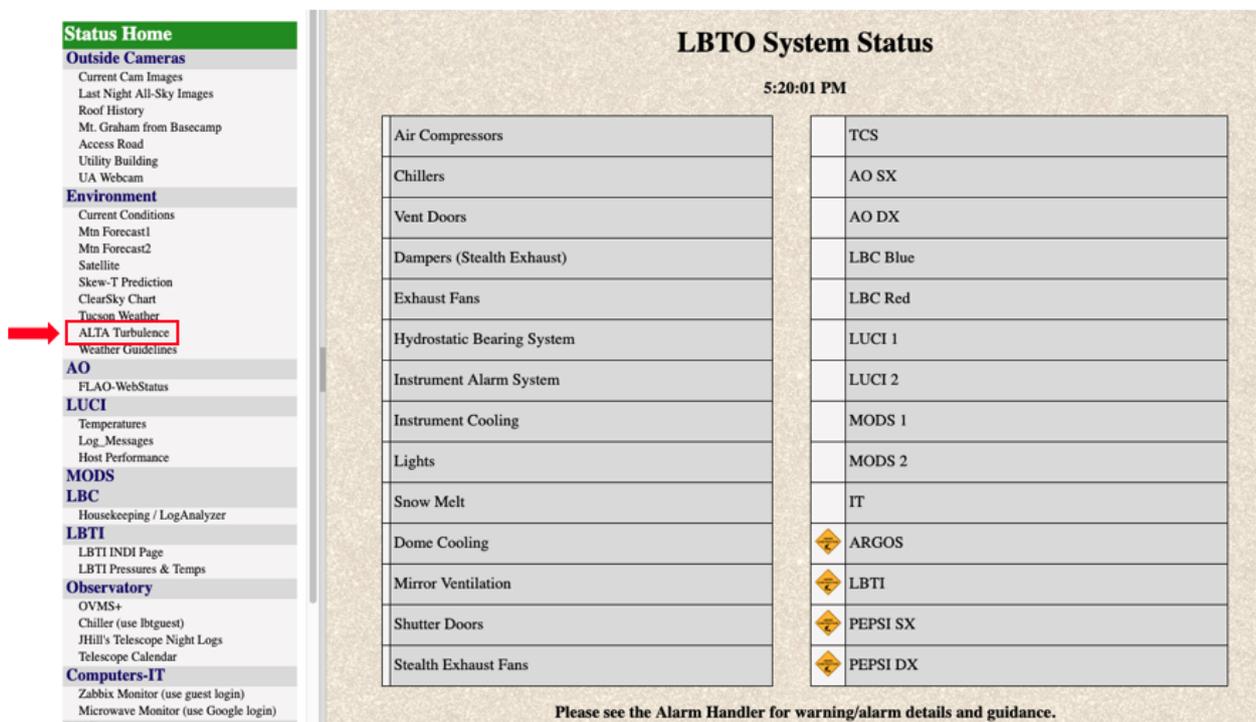
Figure 53: LBTO system status

Fig.54 shows an example of the forecast of the temperature close to the ground all along the night as extracted from the telemetry. The picture shows the forecast at long as well as at short time scale of the temperature.

ALTA data are then injected inside the Science Operation tool. In this perspective Fig.55 shows an example of forecasts at long and short time scales extracted from the telemetry. Besides to the black, red and green lines that represent respectively the forecasts at long and short time scale and the observations with a moved average of 1 hour as reported in the ALTA web page, here are included also with orange dots, the raw observations in real-time. This can be useful in the interval of one hour between a forecast at short time scale and the successive one.
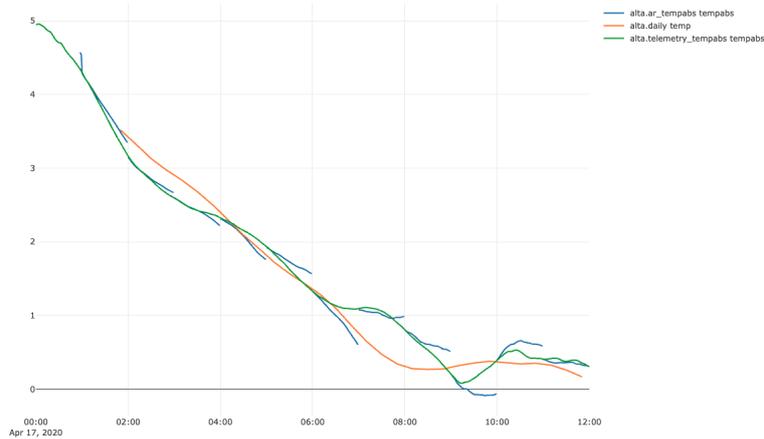
Figure 54: LBTO Telemetry: example of a forecast of the absolute temperature close to the ground as extracted from the telemetry. Green line: observations; Orange line: forecast at long time scale; Blue line: forecast at short time scale (1h).
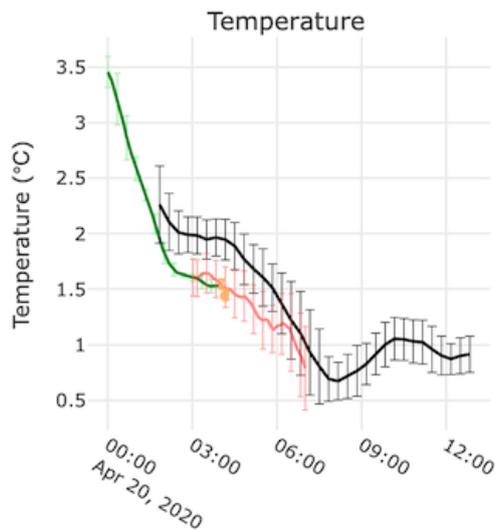
Figure 55: Example of metadata extracted from the telemetry system for the Science Operation tool. Black line: forecast at long time scale; red line: forecast at short time scale; green line: observations filtered; orange dots: raw observations.

7   Achievements not originally planned in the contract

7.1   A new method proposed for the forecast at short time scale

On 2018 we started to work on methods aiming to improve the forecasts performances on short time scales. The goal was to evaluate the possibility to improve the performances of forecasts on time scales of the order of 1h or 2h that are the most critical ones for the science operations and the flexible scheduling. The idea behind was to use filtering techniques with the support of real-time measurements of the parameters that are monitored in situ. Our study lead us to set-up an algorithm based on the autoregressive method (AR). Such a method has been studied and characterised in **Masciadri et al. 2020** [6] and revealed to be extremely promising. The principle implies the simultaneous use of the forecasts at long time scale and the real-time measurements belonging to the present and to a fixed number of nights in the past to produce a more accurate forecast. Once completed the analyses the method has therefore been implemented in the automatic forecast system of the ALTA Center. Such an option can be applied obviously **only** to those parameters for which it is performed a nightly monitoring in situ therefore: temperature, relative humidity, wind speed and direction and seeing.
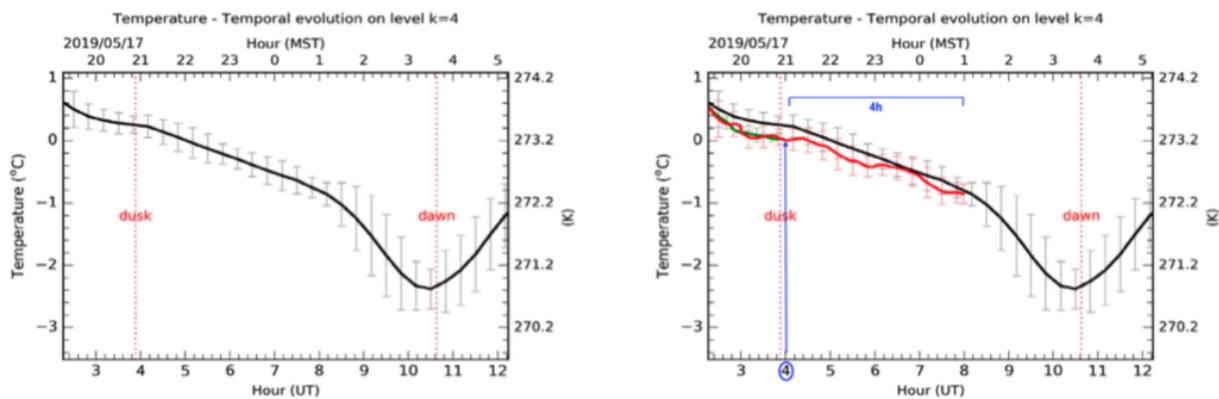
Figure 56:   *Extracted from Masciadri et al. 2020 - Fig.2.* Left: temporal evolution of the forecast of the temperature for the whole night (2019 May 17) at Mt.Graham. The forecast is available at 14:00 MST (local time) of the day before. On the x-axes is reported the time expressed in UT (bottom) and local time (top). Right: temporal evolution of the forecast of the temperature available at 14:00 MST of the day. before (black line); real-time measurements in situ (green line); forecast of the temperature using the AR technique (red line). The latter is calculated at 04:00 UT and extended on the successive 4h (see text).

On March 2019 it has been activated the AR option in the automatic forecast system. Since there the ALTA Center provides nightly forecasts of the different atmospheric parameters at two time scales:

(1) at long time scales i.e. at 14:00 LT for the successive night, option that we call 'standard';

(2) at short time scales that means forecast extended on one up to a few hours and calculated at each full hour of the night.

We refer the reader to the paper [6] for the details of the analysis and discussion. We report here the main concepts and results to permit to appreciate the content of the work.

The method is based on a function that depends on the difference between the real-time observations taken in-situ that we take as a reference (i.e. we assume to be the "truth") and on the forecasts performed by the atmospheric model. When we deal about 'atmospherical model' we are referring to the forecast of the model in standard configuration that is available early in the afternoon of the day before.
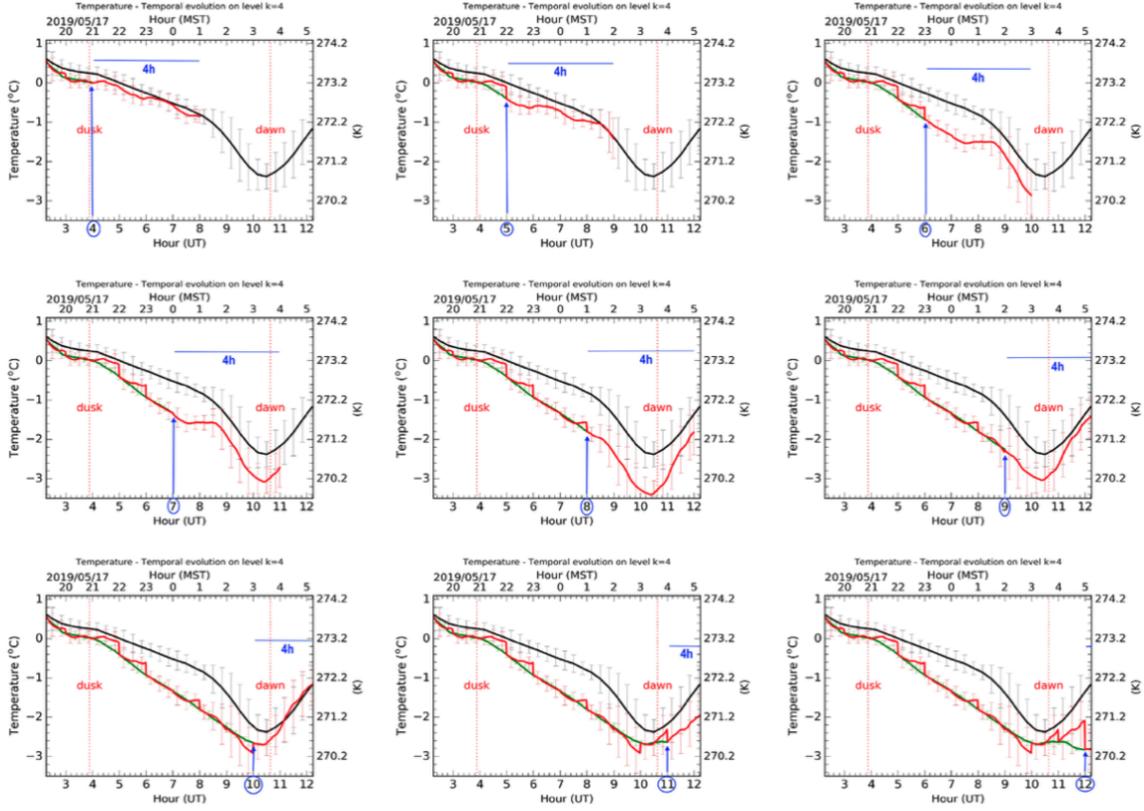
Figure 57: *Extracted from Masciadri et al. 2020 ([6]) - Fig.3*. Temporal sequence of the up-dated forecasts of the temperature with one hour step during the night 2019/05/17. First image on top-left is the situation at 04:00 UT of 2019/05/17, last image on bottom right is the situation at 12:00 UT of 2019/05/17. The sequence is read by rows, from the left to the right. The black line is the forecast of the temperature available at 14:00 UT of the day before. It is therefore always the same in all the pictures. The green-line is the real-time measurements. In each picture the end of the green line end at the time in which the AR forecast is calculated The red-line is the forecast of the temperature obtained with the AR technique. The red line in the last picture (bottom-right) represents the model forecast at 1h for the whole night.

The auto-regressive model (AR) X_{t+1}^* calculated at the (t + 1) is:

$$X_{t+1}^* = M_{t+1} + X_{t+1} \tag{3}$$

where M is the model output at the time (t +1) and the function X at the time (t + 1) depends on the difference between the observations and the atmospherical model outputs calculated on a polinomial function built with the addition of P terms characterised by P coefficient a_i (called regressors) in the form:

$$X_{t+1} = \sum_{i=1}^{P} a_i (OBS_{t-i+1} - MOD_{t-i+1}). \tag{4}$$

where OBS are the real-time measurements and MOD are the atmospheric model outputs in the standard configuration. We refer the readers to Mascaidri et al. 2020 for the discussion on P. We identified an optimal trade-off P=50 for a temporal frequency of 1 minute.
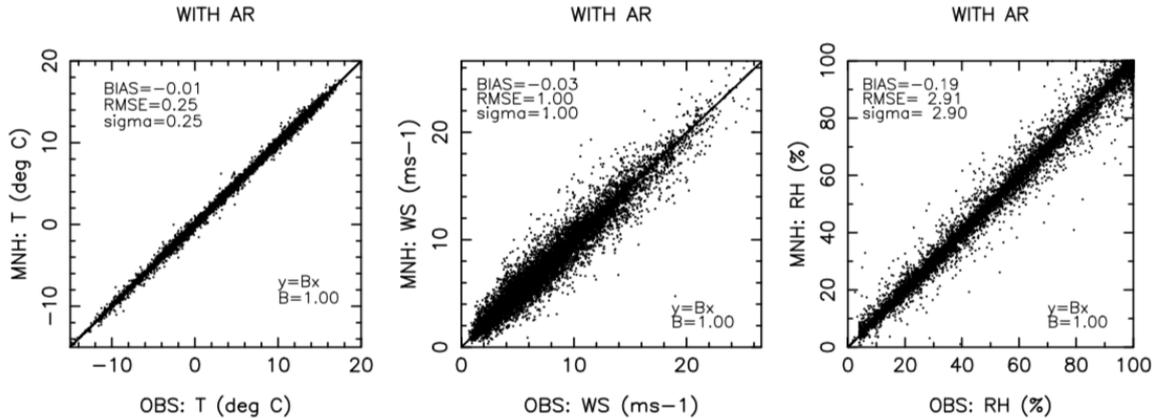
Figure 58: *Extracted from Masciadri et al. 2020 ([6]) - Fig.4.* Scattering plot between observations and AR method outputs for absolute temperature (left), wind speed (centre) and relative humidity (right). Data are treated with a moving average on one hour and resampling on 20 minutes. Number of nights on which the regressors are calculated is N=5.
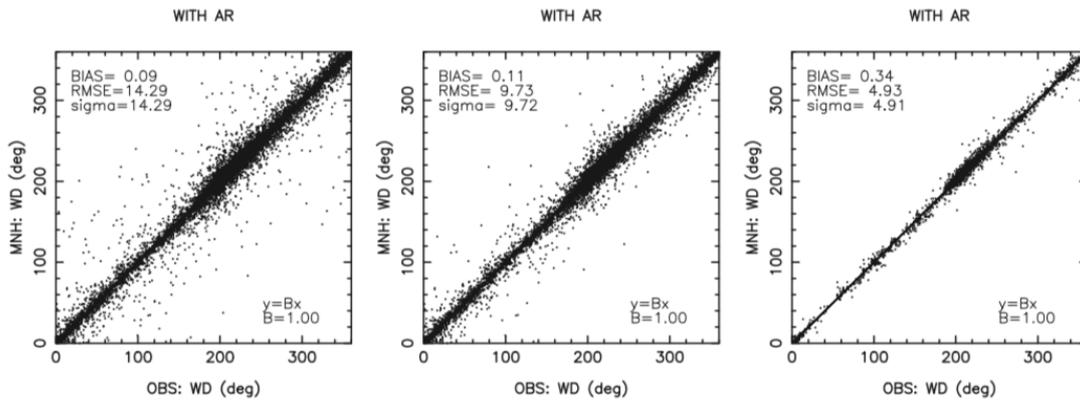
Figure 59: *Extracted from Masciadri et al. 2020 ([6]) - Fig.5.* Scattering plot between observations and AR method outputs for the wind direction (left). Same results but filtering out all cases in which WS is weaker than 3 ms^{-1} (centre) and weaker than 10 ms^{-1} (right).

The values of the 50 regressors is obtained through a Least Mean Square (LSM) method applied to a finite number of nights in the past i.e., for example, the last 3, 4, 5, etc. nights.

Fig.56 shows how the AR method works. At 14:00 LT the ALTA Center displays the forecast at long time scale related to the whole duration of the coming night (black line). The example of Fig.56 indicates the forecast of the temperature. When the night starts, at each full hour is calculated the forecast using the AR method extended on the successive 4 hours (red line). The green line represents the real-time measurements.

Fig.57 shows how it evolves on the time scale of a one night. After the night started, at each full hour the AR forecast of the different parameters extended on the successive four hours is calculated and displayed on the web site. The point with respect to which the forecast is calculated is shifted of one hour all along the night with a frequency of one hour (see the blue arrow in Fig.57). If we look at the last figure on the bottom-right the red line represents the forecast on a time scale of 1h. In the ALTA Center web page at each successive full hour the displayed image is upgraded.

In order to quantify the model performances of the forecasts on one hour time scale using the AR method
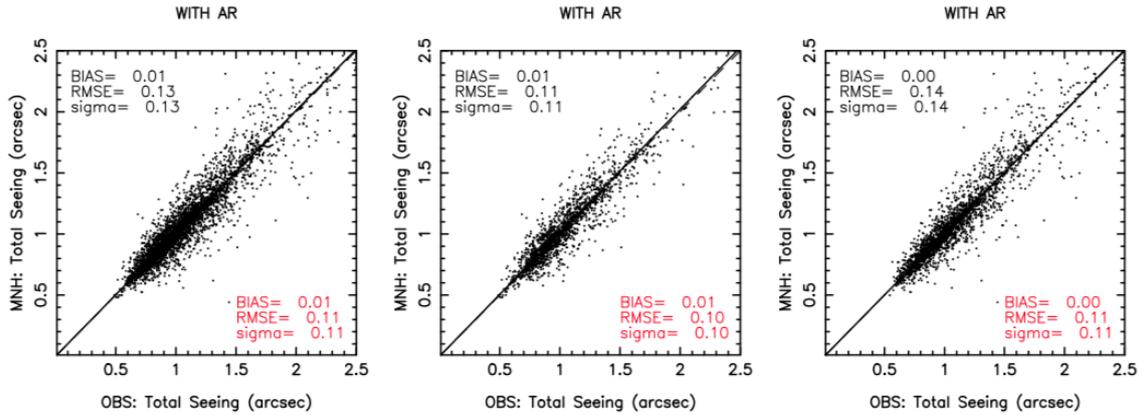
Figure 60: *Extracted from Masciadri et al. 2020 ([6]) - Fig.6.* Scattering plot between observations and AR method outputs for the total seeing calculated on the whole year (left), in the summer period (centre) and in the winter period (right). Summer period is included in the [April-September] interval, winter period in the [October-March] interval. In black results considering all values, in red considering only observations below 1.5" (see discussion in the text).

RMSE	T ($^\circ$ K)	RH (%)	WS (ms^{-1})	WD (> 3ms^{-1}) (degrees)	Seeing (arcsec)
atm. model standard config.	0.98	14.17	2.81	34.71	0.30
AR (@ 1h)	0.25	2.91	1.00	9.73	0.11

Figure 61: *Extracted from Masciadri et al. 2020 ([6]) - Table 2.* RMSE as obtained with the atmospheric model in the standard configuration and as obtained with the AR method on a 1h time scale. In the case of the seeing we considered only seeing below 1.5". This threshold is more than representative for the AO applications and it guarantees a model performances comparable to the dispersion obtained with measurements.

built as we have just described it is necessary to consider a very rich statistical sample because the AR method requires a sequence of data related to successive nights in which it is important to minimise the number of breaks. We considered therefore data of all the nights of the whole year 2018 and we calculated the statistical operators (bias, RMSE and σ) for temperature, relative humidity, wind speed, wind direction and the total seeing. Real-time measurements and outputs of the atmospheric model in standard-configuration related to these parameters have been treated using the same procedure: we first apply a moving average of one hour to filter out the high frequencies and put in evidence the forecast trend, we perform a resampling on a time scale of 20 minutes and we conclude with the calculation of the various statistical operators.

Figure 58 shows the scattering plot related to the temperature (left), the wind speed (centre) and the relative humidity (right) obtained with an AR at a time scale of 1 hour. Figure 59 shows the scattering plot of the WD at the same time scale of 1 hour obtained including all the data (left), filtering out all the data associated to wind speed weaker than 3 ms^{-1} (centre) and filtering out all data having a wind speed weaker than 10 ms^{-1}. We skipped out the data associated to a WS weaker than 3 ms^{-1} because under this condition it is extremely difficult (and meaningless) to quantify the WD because to the high variability of the WD. The central picture of Fig.59 is therefore more representative for the WD than the left one. We skipped-out data weaker than 10 ms^{-1} to quantify the model performances in those cases that are certainly the most critical one for the ground-based

Gain	T	RH	WS	WD	Seeing
AR	3.90	4.90	2.80	3.60	2.70
Persistence	2.40	3.00	1.80	2.40	2.00
AR/persistence	1.63	1.63	1.56	1.50	1.35

Figure 62: *Extracted from Masciadri et al. 2020 ([6]) - Table 3.* Gain obtained for the RMSE for the different atmospheric and astroclimatic parameters using the AR method on a time scale of 1h (first row) and using the method per persistence. (second row). In the third row is reported the gain of the AR with respect to the method per persistence

observations, i.e. those in which the WS is very strong. To conclude, Fig. 60 shows the scattering plot for the seeing in the whole year (left), in the summer [April - September] interval (centre) and winter [October - March] interval (right).

Fig. 61 reports the RMSE obtained for the AR method at a time scale of 1 hour and with the atmospheric model in the standard configuration. We observe that, for all the parameters, the values of RMSE obtained with the AR method at a time scale of 1h are definitely better than for the standard configuration with consistent gains that are variable depending on the parameters between a minimum of a factor 2.7 and a maximum of 4.9 (Fig. 62 - first row).

It remains to consider how to fix the number of nights on which to calculate the regressors. We estimated that the best performances (i.e. the minimum RMSE) is observed for a number N of nights in the past equal to 5. We refer the reader to Masciadri et al. 2020 - Section 5 - Fig.7 for the demonstration. In this condition the gain in RMSE is optimised for the longest interval of time.

In order to appreciate the impact of our method on the gain in performances we compared our approach with the method of persistence. The method per persistence means that, at each full hour, the forecast extended on the successive 4 hours, is obtained by considering the present time measurements as a constant for all its future evolution. Fig.63 shows the RMSE versus the ΔT obtained with the optimised AR method (N=5) and the persistence method. ΔT is the interval of time on which we calculate the forecast. It is clearly visibly that, as expected, even if the use of pure real-time measurements provides an improvement of the forecast performances on short time scales with respect to the standard configuration of the model, the AR method that we propose has definitely a more important gain and better performances for all the atmospheric parameters including the optical turbulence with differences (with respect to the persistence method) that are quantitatively not negligible.

To complete the analysis of the model performances, we finally calculate the contingency tables for each parameter from which we can retrieve the probability of detection (POD), the percentage of correct detection (PC) and the extremely bad detection (EBD). Contingency tables allow for the analysis of the relationship between two or more categorical variables.We refer the readers to [18] for a detailed definition and description of this tool. Here we just remind the principal role of the contingency tables. Given a statistical sample of observations and predictions, the contingency tables permit to calculate the number of times in which observations and predictions fall in the same intervals of values. We used 3×3 tables for all the parameters with exception of the WD that requires a 4×4 table as it is a 2π periodic parameter. Starting from this distribution it is possible to calculate the probability to detect a specific atmospheric parameter in specific intervals of values, the so called POD_i, the percentage of correct detection (PC) and the extremely bad detection (EBD). The thresholds of the intervals are calculated from the climatology of in-situ measurements and they are, usually, the first and third tertiles of the cumulative distribution Fig.64.

Fig. 65, 66, 67, 68 and Fig. 69 report the results of POD_i, PC and EBD for temperature, wind speed, relative humidity, wind direction and seeing in the different configuration: atmospheric model in standard configuration and AR at 1 h time scale. For temperature, WS, RH and seeing, we take i=1,2,3; POD_1 is the probability to detect values smaller than the first tertile; POD_2 is the probability to detect values between the first and
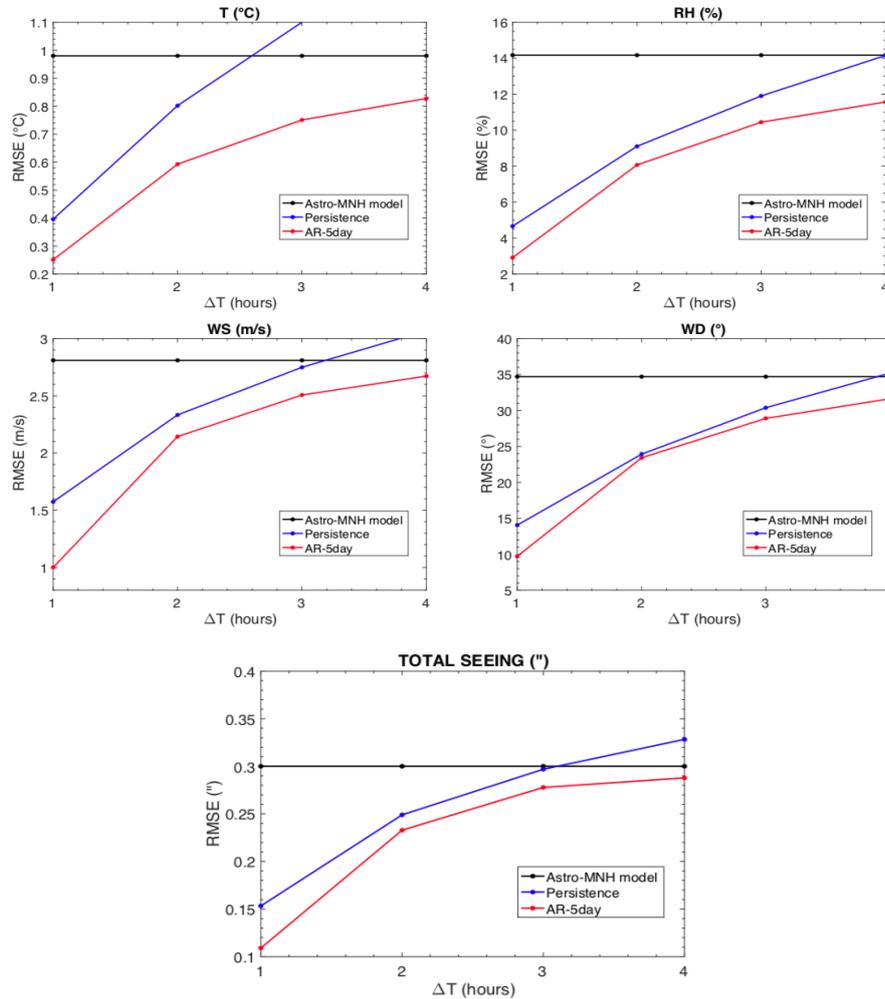
Figure 63: *Extracted from Masciadri et al. 2020 ([6]) - Fig.8.* Dependency of the RMSE of different atmospheric parameters with respect to different ΔT. On the x-axes the 'forecast time' $\Delta T = (T_f - T_i)$ where T_i is the time in which the forecast is calculated and T_f is the time for which the forecast refers to. Example: $\Delta T = 1$ means a forecast at 1 hour calculated at T_i. Red line: the RMSE for the AR method. Blue line: the forecast per persistence. The horizontal black line represents the RMSE calculated with the model in standard configuration (forecast at long time scale).

the third tertiles; POD_3 is the probability to detect values larger than the third tertile. For the WD we take i=1,2,3,4 and POD_1, POD_2, POD_3 and POD_4 are, respectively, the probability to detect a value in the range $[0°, 90°]$, $[90°, 180°]$, $[180°, 270°]$ and $[270°, 360°]$. The same calculation has also been done by rotating the thresholds of $45°$ i.e. $45°$, $135°$ and $225°$ (see [19]). In the case of the seeing, we calculate a contingency table that takes into account an accuracy of 0.2". In reality the dispersion between the seeing measured by different and independent instruments (such as Stereo-SCIDAR and DIMM) can reach values as high as 0.29" [19] but we decided to use 0.2" to be more conservative and because this is a technical specification assumed in some top-class telescopes.

We put the accent on the most relevant result obtained in this analysis and related to the seeing. The most critical POD_1 i.e. the probability to detect a seeing weaker than the first tertile is equal to 81% for the standard configuration and it is equal to 98% for the AR method at 1h time

Table 4. Climatology tertiles calculated on measurements extended on one full solar year (2018) for the absolute temperature T, the wind speed WS, the relative humidity RH, and the seeing.

Param.	1st tert.	Median	3rd ter.
T (°C)	1.00	4.11	8.23
WS (m s^{-1})	5.52	7.15	9.08
RH (%)	31.63	47.48	66.67
Seeing (arcsec)	0.93	1.05	1.20
Seeing (<1.5 arcsec)	0.90	0.99	1.10

Figure 64: *Extracted from Masciadri et al. 2020 ([6]) - Table 4.* Climatology tertiles calculated on measurements extended on one full solar year (2018) for the absolute temperature T, the wind speed WS, the relative humidity RH and the seeing.

	Temperature (T)	
Param.	Forecast the day before (%)	Forecast with AR at 1 h (%)
POD$_1$	96	99
POD$_2$	91	98
POD$_3$	96	99
PC	94	99
EBD	0	0

Figure 65: *Extracted from Masciadri et al. 2020 ([6]) - Table 5.* Model performances in reconstructing the absolute temperature at different time scales: at 14h i.e. when we provide a forecast early in the afternoon of the day (J-1) for the next night, and at 1h with AR. POD$_1$, POD$_2$ and POD$_3$ are the probability of detection related to the intervals: T < 1st tertile, 1st tertile < T < 3rd tertile, T > 3rd tertile. The 1st and tertiles 3rd are shown in Fig. 64.

step. Both are well above the threshold of 33% that is the percentage that corresponds to the random case and the AR method is very close to the saturation in terms of performances. Somehow weaker is the probability to detect the seeing larger than the third tertile (65%) in the standard configuration as the larger is the seeing, the larger is the dispersion between observations and numerical calculation. We have here more space for further improvements of the technique.

The conclusion of this analysis is that the AR method revealed to be extremely efficient in improving the forecasts performances at short time scales. The best improvement is obviously observed at the shortest interval of time ΔT on which the forecast is calculated and it decreases as ΔT increases. We observed that an improvement with respect to the standard forecast is present up to a scale of a few hours (between 4h and 6h) but it varies depending on the parameter. A factor as high as 5 has been observed for the gain in forecast performances.

7.2   Precipitable Water Vapour

The precipitable water vapour (PWV) was not originally included in the list of parameters to be forecasted. This is the reason why we mention it in this part of the report. As it is an atmospherical parameter we preferred to report the results of the work done in this respect in Section 4.1 so to include the PWV together with the other atmospherical parameters.

Param.	Wind speed (WS)	
	Forecast the day before (%)	Forecast with AR at 1 h (%)
POD$_1$	72	91
POD$_2$	48	83
POD$_3$	75	93
PC	65	89
EBD	2	0

Figure 66:   *Extracted from Masciadri et al. 2020 ([6]) - Table 6.* As Fig.65 but for the wind speed (WS).

Param.	Relative humidity (RH)	
	Forecast the day before (%)	Forecast with AR at 1 h (%)
POD$_1$	91	98
POD$_2$	73	95
POD$_3$	71	97
PC	78	97
EBD	1	0

Figure 67:   *Extracted from Masciadri et al. 2020 ([6]) - Table 7.* As Fig.65 but for the relative humidity (RH).

7.3   Equivalent (or effective) wind speed for FLAO, ARGOS and LINC-NIRVANA

On November 2016 we implemented in the ALTA Center a new parameter that is relevant for the three adaptive optics system: FLAO, ARGOS and LINC-NIRVANA. This is called the equivalent velocity. It is a velocity that is called equivalent because it assumes to be equivalent to a unique vertical slab coincident to the vertical slab at which the optical system is sensitive one. The vertical slab depends on the geometry of the optical system. The V_{eq} is extremely critical for the correspondent AO system as it provides us information of the velocity of the turbulence for which the optical system is sensitive to. In the successive sections is reported the analytical expression of the V_{eq} and are shown examples of the V_{eq} in the case of FLAO, ARGOS and LINC-NIRVANA. The forecast of this parameters provides critical informations to control and optimise the respective AO systems.

7.3.1   FLAO

FLAO is the Single Conjugated Adaptive Optics (SCAO) system of LBT. The wind speed at which the system is therefore sensible is the integral of the wind speed of all the turbulence layer developed on the whole atmosphere. Such a velocity is called 'equivalent velocity' (Eq.5), it is defined as an integral of the wind speed weighted by the C_N^2 and normalised by the turbulence developed on the whole atmosphere.

$$V_{eq} = [\frac{\int_{Hmin}^{Hmax} |V(h)|^{5/3} C(h)_N^2 dh}{\int_{Hmin}^{Hmax} C(h)_N^2 dh}]^{3/5} \tag{5}$$

The integral is considered between the primary mirror ($H_{min} = H_{prim}$) and the top of the atmosphere i.e. around $H_{max} = 20$ km. Fig.70 shows the equivalent wind speed V_{eq} temporal evolution between the sunset and the sunrise as indicated in Eq.5 during the night. Astronomical dusk and dawn are shown too. On the x-axis

| | Wind direction (WD: 90°, 180°, and 270°) | |
Param.	Forecast the day before (%)	Forecast with AR at 1 h (%)
POD_1	78	94
POD_2	75	93
POD_3	88	94
POD_4	57	93
PC	81	94
EBD	2	0

Figure 68: *Extracted from Masciadri et al. 2020 ([6]) - Table 8.* As Fig.65 but for the wind direction (WD) using as a thresholds: 90°, 180° and 270°.

| | Seeing (ε) | |
Param.	Forecast the day before (%)	Forecast with AR at 1 h (%)
POD_1	81	99
POD_2	80	97
POD_3	65	98
PC	79	98
EBD	14	1

Figure 69: *Extracted from Masciadri et al. 2020 ([6]) - Table 10.* As Fig.65 but for the seeing (ε). Values calculated assuming an accuracy of 0.2". We considered the seeing < 1.5".

is time in UT (bottom), in MST (top). Raw data points frequency is equal to the model time-step (typically from a fraction of second up to a few seconds depending on the model configuration used). Data points are re-sampled at a frequency of 20 minutes after a 1-hour moving average. The error bars are the sigma over the 20 minutes sampling, computed before the moving average. V_{eq} gives us an information on how fast/slow an AO system has to run. Fig.71 shows the vertical slab of the atmosphere at which FLAO is sensitive to. The V_{eq} corresponds to the effective velocity of the vertical slab indicated in Fig.71. The same parameter will be obviously valid for SOUL when it will be in a definitive run.

7.3.2 ARGOS

ARGOS is the Ground Layer Adaptive Optics (GLAO) system of LBT. The single DM is conjugated at 126 m above the ground. The wind speed that contributes to the V_{eq} is therefore sensible is the integral of the wind speed of each turbulence layer developed inside the depth of field of the optical system weighted by the correspondent C_N^2, normalised by the turbulence developed in the whole depth of field. The total depth of field ΔH (Fig.72) is defined as $\Delta H = 2$ (d/θ) centred at the conjugated plane height, where d is the distance between two effective adjacent actuators projected on the pupil of the telescope and θ is the FOV.

For DM1 $\Delta H_{126m} = [-308,560]$ m = 868 m (Fig.72) where we considered $FOV_{DM1} = 4$ arcmin. The analytical eqaution for ARGOS is the same of that for FLAO (Eq.5) but in this case H_{min} and H_{max} are the extremes of the vertical slabs. Fig.73 shows the equivalent wind speed V_{eq} temporal evolution integrated on the respective depth of field ΔH_i between the sunset and the sunrise as indicated in Eq.5 during the night. Astronomical dusk and dawn are shown too. On the x-axis is time in UT (bottom), in MST (top). Raw data points frequency is equal to the model time-step (typically from a fraction of second up to a few seconds depending on the model
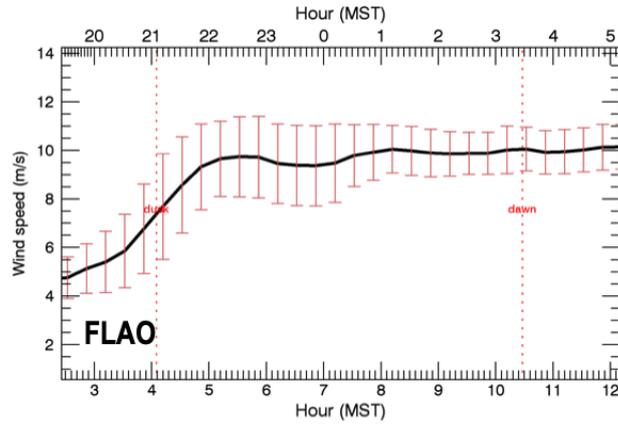
Figure 70: Temporal evolution of the V_{eq} forecasted by the Astro-Meso-Nh model as seen by FLAO between the sunset and the sunrise.
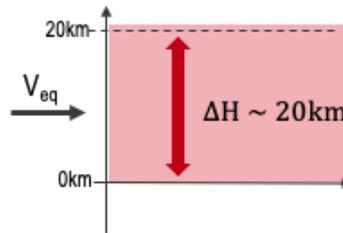
Figure 71: Vertical slab of the atmosphere at which FLAO is sensitive to.

configuration used). Data points are re-sampled at a frequency of 20 minutes after a 1-hour moving average. The error bars are the sigma over the 20 minutes sampling, computed before the moving average. V_{eq} gives us an information on how fast/slow an AO system has to run.
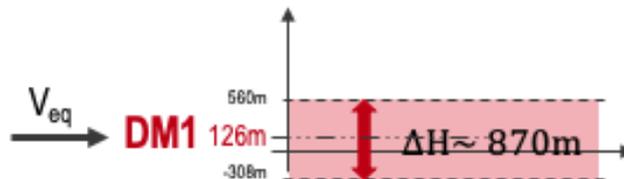
Figure 72: Vertical slab of the atmosphere at which ARGOS is sensitive to.
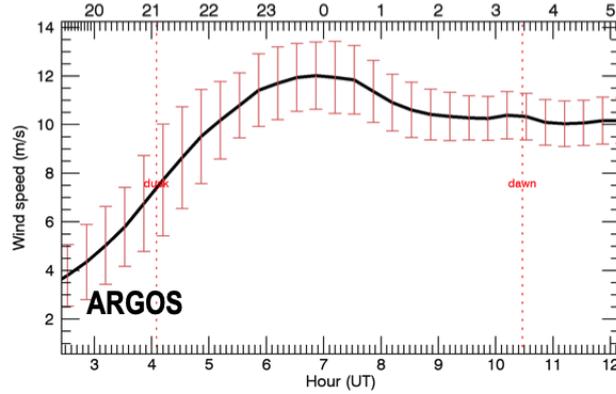
Figure 73: Temporal evolution of the V_{eq} forecasted by the Astro-Meso-Nh model as seen by ARGOS between the sunset and the sunrise.

7.3.3 LINC-NIRVANA

LINC-NIRVANA is the layer-oriented MCAO system of LBT in which the two DMs are conjugated at 126 m and 7.1 km above ground layer. The wind speed at which the system is therefore sensible is the integral of the wind speed of each turbulence layers developed inside the depth of field weighted by the correspondent C_N^2, normalised by the turbulence developed in the whole depth of field (see Eq.5). The total depth of field ΔH is defined as $\Delta H = 2 (d/\theta)$ centred at the conjugated plane height, where d is the distance between two adjacent actuators projected on the pupil (or metapupil) of the telescope and θ is the FOV. In the specific case the depths of field are:

for DM1: $\Delta H_{126m} = [-163, 415]$m = 578 m
for DM2: $\Delta H_{7.1km} = [5072, 9127]$m = 4055 m

where we considered $FOV_{DM1} = 6$ arcmin and $FOV_{DM2} = 2$ arcmin. Fig.74 shows the depth of field of the optical system at the two conjugated heights of 126 m and 7.1 km.

Temporal evolution of the V_{eq} given by Eq.5 where H_{min} and H_{max} are the extremes of the two vertical slabs (Fig.74).

Fig.75 shows the temporal evolution of the equivalent wind speed V_{eq} integrated on the respective depth of field ΔH_i between the sunset and the sunrise as indicated in Eq.5 during the night. Astronomical dusk and dawn are shown too. On the x-axis is time in UT (bottom), in MST (top). Raw data points frequency is equal to the model time-step (typically from a fraction of second up to a few seconds depending on the model configuration used). Data points are re-sampled at a frequency of 20 minutes after a 1-hour moving average. The error bars are the sigma over the 20 minutes sampling, computed before the moving average. V_{eq} gives us an information on how fast/slow an AO system has to run.

7.4   2D wind speed maps for LINC-NIRVANA observations

All the 2D maps of the atmospheric parameters (as well as the astroclimatic parameters) refer to the observation with respect. In other words, the 2D maps of the wind speed at 200 mb represent the component of the wind speed perpendicular to the zenith. This is not a major problem as all the astroclimatic parameters (measured and predicted) are normalised with respect to the zenith. This is done for two major reasons. From one side this approximation is justified by the near-field approximation that from a pragmatic point of view is as if we consider homogeneous horizontal stratifications of turbulence. On the other side if one wishes to compare results obtained with different tools it is fundamental to use the same reference.

Figure 74: Vertical slabs of the atmosphere at which LINC-NIRVANA is sensitive to. Left: DM1. Right: DM2.
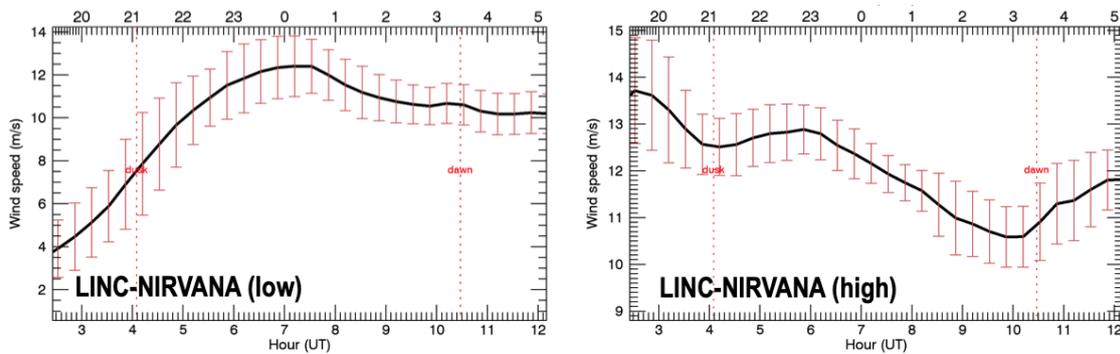
Figure 75: Temporal evolution of the V_{eq} forecasted by the Astro-Meso-Nh model as seen by LINC-NIRVANA and related to the vertical slab associated to DM1 (left) and to the DM2 (right).

When we are dealing about the wind speed it can happen that, for some specific reasons, one is interested in knowing the wind speed map at different angles. This is the case of LINC-NIRVANA. As we have said in Section 7.3 the second DM (DM2) is conjugated at 7.1 km above the ground and for the instrument scientists is important to know the WS component as seen by the WFS when the line of sight is different from zenith. Fig.76 shows how the WS projection on a perpendicular plan to the zenith decreases when the air mass angle increases. Fig.77 shows as an example, the 2D map of the WS projected on a perpendicular plan to the line of sight taken at zenith, and with an air mass of 30° and 60°. It is possible to note that the wind speed changes drastically on the summit of Mt.Graham. In the example shown the WS decreases from something around 14 ms^{-1} at zenith down to 6 ms^{-1} at 60°.

Of course the line of sight might be whatever among 0° and 60°. In order to provide to the instrument scientist an idea of the order of magnitudes of the WS in the volume, we added in ALTA Center the display of the 2D map of the WS$_{7.1km}$ (that is the height at which is conjugated the DM2) projection on the perpendicular direction to the line of sight as seen at zenith and at 30° and 60°.

The WS seen by the WFS plays of course a fundamental role in determining the τ_0 for the instrument for a specific vertical slab. Knowing that:

$$\tau_{0,obs} = r_{0,obs}/V_{eq,obs} \tag{6}$$

and

$$r_{0,obs} = r_{0,zenith} \cdot (\cos \alpha)^{3/5} \tag{7}$$

and

$$V_{eq,obs} = V_{eq,zenith} \cdot \cos \alpha \qquad (8)$$

it follows that:

$$\tau_{0,obs} = \tau_{0,zenith} \cdot (\cos \alpha)^{2/5} \qquad (9)$$

and this tells how fast the AO system has to be tuned to optimised the correction with respect to different lines of sights.
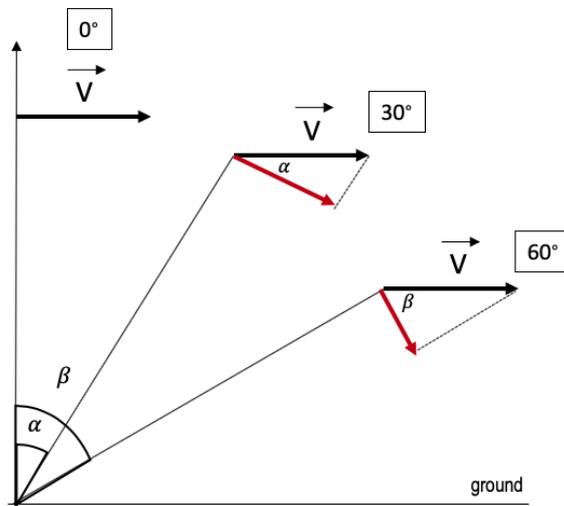
Figure 76:   Toy model showing how the wind speed projected on a plan perpendicular to the zenith changes as the line of sight change.
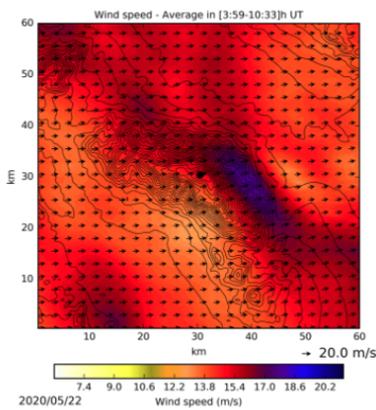
Fig. 4: Wind speed and direction map [60kmx60km] at 7100m above the ground (0° with respect to zenith). Average between dusk and dawn.
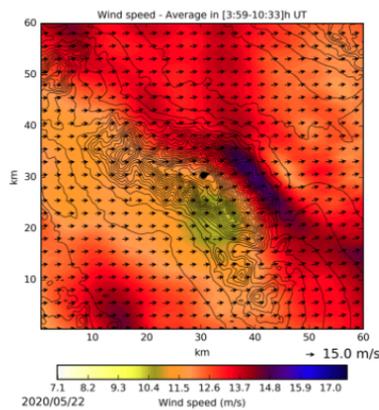
Fig. 5: Wind speed and direction map [60kmx60km] at 6149m above the ground (30° with respect to zenith). Average between dusk and dawn.
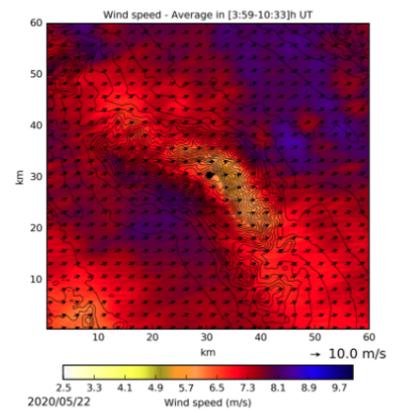
Fig. 6: Wind speed and direction map [60kmx60km] at 3550m above the ground (60° with respect to zenith). Average between dusk and dawn.

Figure 77: Example extracted from ALTA Center. 2D map of the wind speed projected on the perpendicular plan to the zenith as seen at different air mass angles.

8 Publications

ALTA Center: papers produced during the contract and contributions to Workshops/International Meetings/Conferences

Peer-Reviewed Journals

3. Masciadri, E., Martelloni, G., Turchi, A. - *Filtering techniques to enhance optical turbulence forecast performances at short time-scales*, 2020, MNRAS, 492, 140

2. Turchi, A., Masciadri, E., Kerber, F., Martelloni, G. - *Water vapor forecast for VLT and LBT*, 2019, MNRAS, 482, 206

1. Turchi, A., Masciadri, E., Fini, L. - *Forecasting surface layer atmospheric parameters at the LBT site*, 2017, MNRAS, 466, 1925

No Peer-Reviewed Journals

5. Masciadri, E., Turchi, A., Martelloni, G., *New achievements in optical turbulence forecast systems in operational mode* , AO4ELT6, Quebec, Canada, 9-14 June 2019

4. Masciadri, E., Turchi, A., Fini, L., *Optical turbulence forecast in the adaptive optics realm*, 2018, OSA Imaging and Applied Optics Congress, Orlando (US) 25-29 June 2018 (OSA Digital Library JW5I.1.pdf) - <u>Invited Talk</u>

3. Turchi, A., Martelloni, G., Masciadri, E., *Evaluation of filtering techniques to increase the reliability of meteo forecasts for ground-based telescopes*, 2018, Proc. SPIE, Adaptive Optics Systems VI, 10703, id. 107036H

2. Veillet, C., Ashby, D.S., Christou, J., Hill, J., Little, J., Summers, D., Wagner, R.M., Masciadri, E., Turchi, A., - *LBTO's long march to full operation: step 2*, 2016, Proc. SPIE 9910, Observatory Operations: Strategies, Processes, and Systems VI, 99100S, doi: 10.1117/12.2234570

1. Turchi, A., Masciadri, E., Fini, L. - *Forecasts of the atmospherical parameters close to the ground at the LBT site in the context of the ALTA project*, 2016, Proc. SPIE 9909, Adaptive Optics Systems V, 990938, doi: 10.1117/12.2231273

Conferences without proceedings

5. Turchi, A. - Recent development of optical turbulence forecast, ADONI, 16-18 May 2018, Orvieto, Italy

4. Turchi, A. - ALTA project: atmospheric model validation- LBT Users' Meeting, 20-23 June 2017, Florence

3. Masciadri, E. - ALTA Center: an operational system for the forecast of the optical turbulence and atmospheric parameters - LBT Users' Meeting, 20-23 June 2017, Florence

2. Masciadri, E., - Optical Turbulence Forecasts: on-going projects - Workshop on Turbulence Profiling, 21-22 March 2017, Marseille, France

1. Turchi, A. - Alta Project: state of the art, ADONI: 10-12 April 2016, Padova

9 Conclusions

The first five years of contract of ALTA Center project concluded with the accomplishment of the original plan established in the MoU. We set up a complete automatic system that is able to predict a set of fundamental atmospheric parameters relevant for the ground-based astronomy i.e. the temperature, the relative humidity (RH), the wind speed (WS) and direction (WD) and the precipitable water vapour (PWV). Besides, the automatic forecast system has been adapted to forecast the most relevant astroclimatic parameters i.e. the seeing (ε), the wavefront coherence time (τ_0) and the isoplanatic angle (θ_0). All the milestones/objectives described in the original program have been achieved. No major problems have been met with exception of the necessity to develop a dedicated model calibration necessary to be used with the available instrument nightly running in situ to monitor the optical turbulence (i.e. a Differential Image Motion Monitor - DIMM).

In order to act as a forecast tool a dedicated web-site has been developed for ALTA Center and it has been organised following a sort of reference baseline that should answer to the necessities of instrument scientists and astronomers. The web site is completed with a dedicated on-line tutoring that allows an autonomous use of the web site.

ALTA Center displays nightly the forecast of the above cited parameters in different formats. More precisely in the form of a simple temporal evolution of an atmospheric parameter forecasted on the summit of Mt.Graham in a predefined specific point (for example the temporal evolution of atmospheric parameters at a few tens of meter a.g.l. where monitors of the different parameters are constantly running), of a temporal evolution of vertical profiles of atmospherical parameters on the whole atmosphere (i.e. relevant for astronomical application therefore around 20 km), of an average of the vertical profiles during a whole night and in the three main parts of the night, or in the form of 2D maps of the atmospherical parameters such as the wind speed and direction at 200 mb or close to the ground. For what concerns the optical turbulence i.e. the C_N^2 it is treated as a standard atmospheric parameter therefore we can access to the temporal evolution of the vertical profile all along the night on the whole 20 km and in the first 2 km above the ground. At the same way, ALTA provides the average of the C_N^2 on the three different parts of the night with associated standard deviation. For what concerns the integrated astroclimatic parameters ALTA Center provides the temporal evolution of seeing θ_0 and τ_0 as well as the contributions in the boundary layer and in the free atmosphere (for seeing and τ_0). At the same time ALTA delivers also 2D maps of those astroclimatic parameters extended on a surface a few kilometers around the summit of Mt.Graham. A detailed list of outputs can be found in Section 3.1.5.

The automatic system is auto-consistent. Initialisation and forcing data come from the ECMWF which provides initialisation data through a yearly contract. The ALTA Center delivers nightly forecasts of all the mentioned parameters that are accessible to the whole LBT Consortium through a password[8]. Forecasts of all the parameters related to the previous three nights are freely accessible by everybody in the world. Part of the forecasts outputs in ASCII formats are nightly automatically transferred to LBTO and injected in the LBTO science operation tool conceived to manage the astronomical observations (see Section 6).

Model forecasts have been validated for all the atmospheric parameters and model performances have been quantified using different figures of merit such as the classical statistical operators bias, RMSE and σ and contingency tables with annexed parameters such as the percent of correct detection (PC), probability of detection (POD$_i$) and probability of extremely bad detection (EBD) (see Section 4). Two papers have been published on peer reviewed journals on this topic: **Turchi et al. 2017** [7] and **Turchi et al. 2019** [11]. For the optical turbulence we developed a new model calibration for the Astro-Meso-Nh model and we validated the model for this parameter using a similar approach used for the atmospherical parameters (see Section 5). Concerning the optical turbulence we could validated only the seeing as there are not at present in situ monitors that can provide real-time measurements of the isoplanatic angle (θ_0) and the wavefront coherence time (τ_0).

More recently we developed a new method aiming to improve the model performances on short time scale (i.e. from 1h to a few hours). The principle of the method as well as its efficiency and validation has been described and published on a peer reviewed journal (**Masciadri et al. 2020** [6]). Afterwards the method has been implemented in the operational automatic system of ALTA Center (See Section 7). The method is based on the application of an autoregressive technique (AR) and takes into account simultaneous forecasts provided

---

[8]The protection of data are imposed by a licence of the ECMWF products. Only data related to the coming night are protected.

with the atmospheric model and real-time measurements of the different parameters extended on the past up to a few days. Of course the method can be applied **only** to those parameters that are systematically monitored in situ. Since March 2019 the ALTA Center system delivers therefore forecasts of temperature, wind speed and direction, relative humidity and seeing at two time scales:

1. Forecast at long time scales: we mean with that the forecasts displayed early afternoon (14 LT) related to the whole coming night - black-line in Fig.11

2. Forecast at short time scales: when the night starts, at each full hour ALTA provides a forecast of the main parameters extended on the successive four hours. These forecasts are up-graded each full hours during the nights - red line in Fig.11.

Such a technique permits to improve by a not negligible factor the accuracy of the predictions. In Table 2 are reported the RMSE related to the different parameters obtained on a time scale of 1h with the AR method and on a standard configuration i.e. for forecasts at long time scale[9]. Results have been calculated on a sample of 365 nights therefore a whole complete year ([6]). Table 3 - Table 8 reports the probability of detection (POD_i) the percent of correction (PC) and the Extremely Bad Detection (EBD) or all the parameters for which it is possible to apply the AR method. In Section 7 a detailed description of these results.

We highlight the fact that, using the AR method, we find a RMSE for the seeing of 0.11 arcsec and a probability to detect the seeing inferior to the first tertile equal to 99% on a time scale of 1h. Such a kind of RMSE is even better than the accuracy with which at present one can hope to estimate the seeing that is hardly better than 0.2 arcsec. Besides, it is worth to note that with such a very small RMSE in predicting the temperature close to the ground (RMSE = 0.98 °C at long time scales and RMSE = 0.25 °C at short time scales) the elimination of the dome seeing through a thermalisation of the primary mirror temperature and the atmosphere inside the dome with respect to the external temperature is not a chimera anymore, as claimed by Racine 1991 [20]. For what concerns the wind speed we calculated that, when the WS > 10 ms^{-1} the $\sigma = 1.2$ ms^{-1}. The strong wind speed, i.e. the main causes of the adaptive secondary and telescope vibrations, can be forecasted therefore with an accuracy of around 1ms^{-1}. If we consider alla the values of WS without restrictions the RMSE =0.58 ms-1. For what concerns the wind direction (WD) we observe that a RMSE = 34.71° at long time scales and a RMSE = 9.73° at short time scales correspond to a $RMSE_{rel}$ = RMSE / 180° = 19% and a $RMSE_{rel}$ = 5% respectively for the long and short time scales. The wind direction can therefore be detected with an extremely high accuracy. This should allow an efficient managing of the science operations as it permits to identify the wind direction in presence of strong wind speed and avoid the line of sights that should look at the wind blowing.

At our knowledge the ALTA Center is the first tool in the world, at least in the astronomical context, that is able to provide forecasts of atmospherical and astroclimatic parameters at different time scales as those indicated and the first tool that proved to be able to achieve performances such as those we obtained with the AR method in this field of application.

What about the method/system of forecast of atmospheric and astroclimatic parameters implemented in ALTA Center ? Are results obtained satisfactory ? Do we have to push further away ?

To answer to these questions we highlight the main motivational principle that lead our work. The approach we intend to follow is very pragmatic. The criterium used is that an achievement is satisfactory if it answers to requirements/necessities.

Here the state of the art:

1. The atmospheric models are very attractive as they directly solve the Navier Stokes hydrodynamic equations governing the atmospheric flow evolution and they are able to retrieve the spatio-temporal evolution of the

---

[9]Forecasts done at 14:00 LT for the successive night

Parameter	T	RH	WS	WD ($> 3\text{ms}^{-1}$)	WD ($> 10\text{ms}^{-1}$)	Seeing
	(° K)	(%)	(ms^{-1})	(degrees)	(degrees)	(arcsec)
RMSE on long time scale	0.98	14.17	2.81	34.71	19.35	0.30
RMSE with AR (@ 1h)	0.25	2.91	1.00	9.73	4.93	0.11

Table 2: RMSE of the forecast as obtained with the atmospheric model in the standard configuration (first row) and as obtained with the AR method on a 1h time scale (second row). In the case of the seeing we considered only seeing below 1.5 arcsec. This threshold is more than representative for the AO applications and it guarantees a model performances comparable to the dispersion obtained with measurements. We highlight the fact that, RMSE = 0.13 arcsec for all values of the seeing (without filtering) using the AR method.

atmospheric flow. The turbulence, frequently triggered by sudden thermo-dynamic instabilities is therefore in principle well placed to be detected by such an approach. We know that mesoscale models such as the Astro-Meso-Nh model implemented in ALTA Center provide better performances than General Circulation Models for atmospheric parameters. As an example, we proved that we gain a factor 2 in predicting the PWV with respect to the GCMs of the ECMWF (the IFS model in the HRES configuration) that is the GCM with the highest resolution at present time in the world (see **Turchi et al. 2019** [11]). Moreover we can state that the GCMs are not suitable to forecast the optical turbulence because of a too low resolution [19].

2. We proved that the AR method that we proposed in **Masciadri et al. 2020** [6] and it is based on an autoregressive technique, provides consistently better results than those obtained with the method of prediction by persistence that uses only real-time measurements. More precisely the AR method revealed to be at present the most performant technique. We can not exclude that other techniques might obtain similar or even better performances. It is indeed our intention to investigate different approaches such as machine learning or Artificial Neural Networking (ANN) taking advantage of real-time measurements in situ even if it is worth to say that performances achieved at present on forecasts at short time scales (from 1h to 2h) are already very satisfactory from a quantitative point of view (see Table 3 - Table 8) and very close to the intrinsic limits. For example, the probability to detect a seeing inferior to the first tertile on a time scale of 1h is of the order of 99%.

3. Predictions at long time scale (i.e. forecasts calculated at around 14:00 LT for the successive night) however still show space for improvements. We are particularly interested on the optical turbulence. A probability of detection of the seeing inferior to the first tertile equal to 80% (assuming an intrinsic accuracy of 0.2 arcsec) is really encouraging but here we have space to increase the model performances. The fields in which it is significative to invest on are the C_N^2 algorithms and the initialisation and forcing data.

We remember that the ALTA Center contract lead so far to the publication of three papers on peer-reviewed journals. See details in Section 8.

Temperature (T)		
Param.	Forecast	Forecast with AR
	the day before (%)	@ 1h (%)
POD$_1$	96	99
POD$_2$	91	98
POD$_3$	96	99
PC	94	99
EBD	0	0

Table 3: Model performances in reconstructing the **absolute temperature (T)** at different time scales: at 14h i.e. when we provide a forecast early in the afternoon of the day (J-1) for the next night, and at 1h with AR. POD$_1$, POD$_2$ and POD$_3$ are the probability of detection related to the intervals: T $< 1^{st}$ tertile, 1st tertile $<$ T $< 3^{rd}$ tertile, T $> 3^{rd}$ tertile. See Section 7 for the 1st and tertiles 3rd.

Wind Speed (WS)		
Param.	Forecast	Forecast with AR
	the day before (%)	@ 1h (%)
POD$_1$	72	91
POD$_2$	48	83
POD$_3$	75	93
PC	65	89
EBD	2	0

Table 4: As Table 3 but for the **wind speed (WS)**.

Relative Humidity (RH)		
Param.	Forecast	Forecast with AR
	the day before (%)	@ 1h (%)
POD$_1$	91	98
POD$_2$	73	95
POD$_3$	71	97
PC	78	97
EBD	1	0

Table 5: As Table 3 but for the **relative humidity (RH)**.

Wind direction (WD: 90°, 180° and 270°)		
Param.	Forecast	Forecast with AR
	the day before (%)	@ 1h (%)
POD$_1$	78	94
POD$_2$	75	93
POD$_3$	88	94
POD$_4$	57	93
PC	81	94
EBD	2	0

Table 6: As Table 3 but for the **wind direction (WD)** using as a thresholds: 90°, 180° and 270°.

Wind direction (WD: 45°, 135° and 225°)		
Param.	Forecast the day before (%)	Forecast with AR @ 1h (%)
POD$_1$	75	94
POD$_2$	62	93
POD$_3$	71	94
POD$_4$	84	93
PC	74	94
EBD	1	0

Table 7: As Table 3 but for the **wind direction (WD)** using as a thresholds: 45°, 135° and 225°.

Seeing (ε)		
Param.	Forecast the day before (%)	Forecast with AR @ 1h (%)
POD$_1$	81	99
POD$_2$	80	97
POD$_3$	65	98
PC	79	98
EBD	14	1

Table 8: As Table 3 but for the **seeing (ε)**. Values calculated assuming an accuracy of 0.2". We considered the seeing < 1.5".

9.1   Perspectives

So far at Mt.Graham there are no monitors that can provide real-time measurements of the isoplanatic angle (θ_0) and the wavefront coherence time (τ_0). This is the main reason why we could not validate the model with respect to these parameters. However, in the LBTO plans, it is foreseen the implementation in situ of a new generation of Multi Aperture Scintillation Sensor (MASS) that is under development. Such an instrument should permit to first validate the model and, afterwards, to extend the AR forecast method at 1h step also to θ_0 and τ_0. This is extremely important for a set of instruments supported by AO that are running at present such as LUCI with the GLAO system ARGOS [21] and the Large Binocular Telescope Interferometry (LBTI) [22] or those that are planned for the near future such as SHARK-VIS [23], SHARK-NIR [24], iLocator [25] that will be supported by SOUL [26], the AO system that will replace FLAO.

At LBTO is also under development a second DIMM that is supposed to be placed outside the dome. The fact to have two DIMMs, one outside and one inside the dome will permits first to retrieve a better comprehension of the seeing close to the ground and inside the dome. Secondly, it will permit us to perform a double model calibration by taking into account both DIMMs and to define a better use of the seeing forecasts in order to support the observations.

At the same time, also an instrument providing real-time measurements of the PWV such as LHATPRO [12] is under evaluation as it should permit an upgrade of the forecasts at short time scale of a parameter such as PWV that is critical for LBTI scientific programs such as those using the nulling interferometry in N band - see HOST project [27] looking for exozodiacal dust near the habitable zone around nearby, main-sequence stars. The utility of such an instrument is not really for the model validation as we could in any case provide a consistent demonstration of the reliability of the forecasts [11]. On the other side the access to real-time measurements should permit the implementation of the AR method on a short time scale. We have recently proven [28] that for the PWV at VLT it is possible to achieve with the AR mode a gain of a factor 8 with respect to the standard forecast method. In particular we achieved a forecast accuracy of 0.04 mm for PWV ≤ 1 mm at 1h. This should permit to isolate the very best conditions of Mt.Graham in terms of water vapour with a high level of accuracy to perform the most challenging scientific programs limited by the PWV.

The AR method also opens to exciting new perspectives as the possibility to improve the forecast accuracy on short time scale might be applied directly to OT vertical distribution with incredibly important impacts particularly on the WFAO where the knowledge of the position of the turbulence layers is crucial. It should be indeed possible to forecast directly the turbulent layers position and strength with expected high accuracy. This is not part of ALTA Center project but it is certainly a topic on which we intend to investigate.

For what concerns the perspectives and the next steps for ALTA there are different actions to be carried out:

From one side it is important a refurbishment of the servers i.e. the hardware supporting the automatic forecast system. When ALTA has been conceived it was figured out to check and to refurbish the servers park on a time scale of roughly five years to take into account the typical lifetime of hardware. Assuming the natural evolution of the architectures and their performances, the refurbishment matches also the interest in improving the model performances. In agreement with the LBTO Director we already performed an investigation aiming to identify the optimal choice for the servers on the base of the best added value/cost ratio. We identified a server that will permit to take initialisation data calculated 12h closest to the time of interest (i.e. to shorten the interval of time between the calculation of the initialisation data and time of display the results). That will definitely permit to improve the model performances. Details will be treated on the MoU related to the renewed contract of ALTA extended on the next five years.

From another side there is a set of actions whose aim is that to support a continuous evolution of the ALTA system.

Part of these actions are related to what is called maintenance of the system that includes, for example, the upgrade of the master version of the atmospherical model and phasing of the OT code to the master atmospheric

code, maintenance of the phasing between initialisation data coming from the General Circulation Model (in our case the ECMWF) and the ALTA system, calculations of trends on climatological time scale, managing of the web ALTA site and many other issues that is is not possible to anticipate as they are, by definition, not predictable. This is the normal activity required to manage the ALTA Center tool aiming to support the science operations of LBTO.

A last set of actions are addressed to improve the performances of the ALTA system or in adding new outputs for ALTA or in performing further analysis. For example AO measurements available in situ from SOUL will permit us to retrieve insights on the seeing that we want to reconstruct and this will put us in better conditions to use DIMM and SOUL measurements to optimise the forecasts of the turbulence as seen by the AO system. We will be able also to provide further model outputs not yet implemented in the system. These actions require a dedicated work that is in definition in agreement with the LBTO Director and it will be subject of a new MoU for the period [2020-2025].

10   Acknowledgements

References

[1] Veillet, C., Ashby, D.S., Christou, J., Hill, J., Little, J., Summers, D., Wagner, R.M., Masciadri, E., Turchi, A., SPIE Proc., Observatory Operations: Strategies, Processes, and Systems VI, 99100S, doi: 10.1117/12.2234570

[2] Lafore J.-P., Stein, J., Asencio, N. et al., 1998, Annales Geophysicae, 16, 90

[3] Lac et al., 2018, Annales Geosci. Model Dev., 11, 1929

[4] Masciadri, E., Vernin, J., Bougeault, P., 1999, A&ASS, 137, 185

[5] Masciadri, E., PhD Thesis, Departement d'Astrophysique - Université de Nice-Sophia Antipolis, Nice, France Caracterisation et prevision de la turbulence optique par un modele atmospherique non-hydrostatique: application a l'haute resolution angulaire

[6] Masciadri, E., Turchi, A., Martelloni, G., 2020, MNRAS, 492, 140

[7] Turchi, A., Masciadri, E., Fini, L., 2017, MNRAS, 466, 1925

[8] Masciadri, E., Stoesz, J., Lascaux, F, Hagelin, S, 2010, MNRAS, 404, 144

[9] Turchi, A., Masciadri, E., Fini, L., 2017, SPIE 9909, Adaptive Optics Systems V, 990938, doi: 10.1117/12.2231273

[10] Carrasco, E., Avila R., Erasmus A., Djorgovski S. G., Walker A. R., Blum R., 2017, PASP, 129, 973

[11] Turchi, A., Masciadri, E., Kerber, F., Martelloni, G., 2019, MNRAS, 482, 206

[12] Kerber F. et al., 2012, Proc. SPIE , Ground-based and Airborne Instrumentation for Astronomy IV, 8448, 84463N

[13] Mascaidri, E. & Jabouille, P., 2001, A&A, 376, 727

[14] Masciadri, E., Avila, R., Sanchez, L.,J., 2004, RMxAA, 39, 249

[15] Cherubini, T., Businger, S., Lyman, R., Chun, M., 2008, Journ. of Appl. Met. and Clim., 47, 1140

[16] Hagelin, S., Masciadri, E., Lascaux, F., 2011, MNRAS, 412, 2695

[17] Masciadri, E., Lascaux, F., Turchi, A., Fini, L, 2017, MNRAS, 466, 520

[18] Lascaux, F., Masciadri, E., Fini, L, 2015, MNRAS, 449, 1664

[19] Masciadri, E., Turchi, A., Martelloni, G., AO4ELT6, Quebec City, 9-14 June 2019, arXiv:1911.02819

[20] Racine, R., 1991, PASP, 103, 1020

[21] Rabien, S., Angel, R., Barl. L., et al., A&A, 621, A4

[22] Hinz, P. et al., 2016, Proc. SPIE 9907, Optical and Infrared Interferometry and Imaging V, 990704

[23] Pedichini, F., Ambrosino, F., Centrone, M., et al., 2016, Proc. SPIE 9908, Ground-based and Airborne Instrumentation for Astronomy VI, 990832

[24] Farinato, J., Agapito, G., Bacciotti, F., et al., 2018, Proc. SPIE 10703, Adaptive Optics Systems VI, 107030E

[25] Crepp, J., Crass, J., King, D., et al., 2016, Proc. SPIE 9908, Ground-based and Airborne Instrumentation for Astronomy VI, 990819

[26] Pinna, E., Esposito, S., Hinz, P, et al., 2016, Proc. SPIE 9909, Adaptive Optics Systems V, 99093V

[27] Ertel, Defrere, D., Hinz, P., et al. 2018, AJ, 155, Issue 5, article id. 194

[28] Turchi, A., Masciadri, E., Pathak, P, Kasper, M., 2020, MNRAS, submitted